Superexchange Electron Tunneling Mediated by Solvent Molecules: Pulsed Electron Paramagnetic Resonance Study on Electronic Coupling in Solvent-Separated Radical Ion Pairs†

Yasuhiro Kobori*
Department of Chemistry, University of Chicago, Chicago, Illinois 60637

Tomoaki Yago, Kimio Akiyama, and Shozo Tero-Kubota*
Institute of Multidisciplinary Research for Advanced Materials, Tohoku University, Katahira 2-1-1, Aobaku, Sendai 980-8577, Japan

Hirofumi Sato
Department of Molecular Engineering, Kyoto University, Sakyo-ku, Kyoto 606-8501, Japan

Fumio Hirata
Department of Theoretical Studies, Institute of Molecular Science and School of Mathematical and Physical Science, The Graduate University for Advanced Studies, Okazaki 444-8585, Japan

James R. Norris, Jr.*
Department of Chemistry and Institute of Biophysical Dynamics, University of Chicago, Chicago, Illinois 60637

Received: September 30, 2003; In Final Form: January 5, 2004

Nanosecond pulsed electron paramagnetic resonance spectroscopy is applied to characterize exponential decay constants (β) of the squared electronic coupling matrix element (V_{DA}^2) in transient, solvent-separated radical ion pairs (RIP) composed of quinone anions and several cation radicals in aprotic liquid solutions of *N*,*N*-dimethylformamide, DMSO, and benzonitrile. The distance dependence of singlet−triplet energy splitting ($2J$) is shown to be described by β in V_{DA} for charge-recombination processes. We show that the radical pair mechanism (RPM) electron spin polarization (P_{RPM}) is quite sensitive to β. The β value is characterized by using the stochastic Liouville equation to fit the experimental P_{RPM} values. The β values (from 0.8 to 1.0 Å^{-1}) manifest that V_{DA} is governed by the superexchange mechanism mediated by the intervening solvent molecules from a result that the β increases with increasing the tunneling energy gap (ΔG_{eff}) for solvent oxidation or reduction in several intermolecular electron-transfer systems. We propose a simple three-dimensional model of V_{DA}, in which the through-solvent tunneling pathways are exponentially increased with the increase in the intermolecular distance in bulk, condensed media. This model explains the ΔG_{eff} dependence of β, including the data previously reported on the charge-transfer reactions both in liquid and frozen (77 K) solutions. Effective solvent−solvent coupling is estimated to be $\upsilon_B \approx 850$ cm^{-1} at a mean nearest-neighbor distance of 5.7 Å. This relatively large magnitude of υ_B may agree with dynamical amplifications of the effective coupling by low-frequency motions of the mediators as reported in charge-transfer reactions in biological systems. (Balabin, I. A.; Onuchic, J. *Science* **2000**, *290*, 114 and Troisi, A.; Orlandi, G. *J. Phys. Chem. B* **2002**, *106*, 2093.)

I. Introduction

Electron transfer (ET) is one of the most fundamental chemical reactions and plays an important role in a wide variety of biological[1] and nanomaterial systems. Considerable interest has been directed to long-range ET reactions in the nanometer scale.[1−9] The rate of long-range, nonadiabatic ET is described as follows[10,11]

$$k_{ET} = \frac{2\pi}{\hbar} |V_{DA}|^2 (\text{FCWDS}) \quad (1)$$

where V_{DA} is the electronic coupling matrix element and FCWDS represents the vibronic Franck−Condon weighted density of states of the electron donor (D)−acceptor (A) system. Solvent molecules play significant roles in determining the long-range ET efficiency in condensed media. Marcus theory has explained how the solvent reorganization energy (λ_s) contributes to the potential barrier and thus affects FCWDS for the ET processes.[10,11] Solvent molecules have also been considered to affect V_{DA}.[12,13] Miller et al. investigated the center-to-center distance (r) dependence of k_{ET} in frozen rigid matrixes to

† Part of the special issue "Gerald Small Festschrift".

* Authors to whom correspondence may be addressed. Phone: +1 (773) 702 9646 (Y.K.); +1 (773) 702 7864 (J.R.N.); +81 (22) 217 5612 (S.T.-K.). Fax: +1 (773) 702 0805 (Y.K.); +1 (773) 702 0805 (J.R.N.); +81 (22) 217 5612 (S.T.-K.). E-mail: ykobori1124@hotmail.com (Y.K.); jrnorris@uchicago.edu (J.R.N.); tero@tagen.tohoku.ac.jp (S.T.-K.).

10.1021/jp036925t CCC: $27.50
Published on Web 03/31/2004

characterize the r dependence of V_{DA}[2].[14] The distance dependence of V_{DA} has been expressed using the exponential decay constant of β as follows[11]

$$V_{DA}(r) = V_0 \exp\left\{-\frac{\beta(r-d)}{2}\right\} \quad (2)$$

where $V_0 = V_{DA}(d)$. Miller et al. suggested that the superexchange mechanism[15] through the oxidized or the reduced state of the intervening solvent molecules may be applicable for long-range ET reactions.[12] Numerous studies have been performed on the mechanism of V_{DA} for several bridged D−A systems. The superexchange mechanism has been discussed for covalently linked D−A molecules,[2,13,16−20] DNA,[6,8,9,21−34] and several ET systems in proteins;[1,4,35−37] the bonded and nonbonded contacts influence the bridge-mediated coupling between the D and A electronic states.

Despite the great importance of understanding the role of the solvent molecules for the electron coupling matrix element in the condensed media,[13,17] only a few experimental studies have been done to characterize the r dependence of V_{DA} in the intermolecular ET systems.[1,37−42] In liquid solvents, β values ranging from 0.9 to 1.1 Å^{-1} have been obtained in nonexponential decay analyses of intermolecular fluorescence quenching by ET.[38−41] However, a detailed mechanism has not been discussed for the β values to understand how *intervening solvent molecules mediate ET in the long-range intermolecular systems*, in which the solute molecules are flexibly separated by each other.[20]

Concerning solvent-separated radical ion pairs (RIP) produced via intermolecular, photoinduced charge separation (CS) reactions, the energy gap ($2J = E_S - E_T$) between the singlet (S) and triplet (T_0) states has been shown to be dominated by charge-transfer interactions (J_{CT}); J_{CT} is determined by V_{DA} via the charge-recombination configurations in accordance with the Marcus theory.[18,43−48] Since the β determines the distance dependence of $2J$,[18,47−49] the β strongly influences chemically induced dynamic electron polarization (CIDEP)[50−54] created through the spin interactions within transient RIPs. During diffusional motion on the S and T_0 potential surfaces, radical pair mechanism (RPM)[54−58] electron spin polarization is created on ion radicals due to the S−T_0 state mixing taking place around the center-to-center intermolecular distance of 12 Å (in the case of $\beta = 1$ Å^{-1}),[59−61] where the magnitude of $2J$ is comparable to that of the hyperfine coupling (typically ca. 10^8 rad/s). When the β value becomes smaller, $2J$ is a more long-range interaction, resulting in longer effective RPM generation distance (r_{eff}).[61] In the previous study, β value dependences of the RPM polarization were theoretically calculated using a simple diffusion model analysis of the stochastic Liouville equation (SLE) while taking into account the J_{CT} mechanism.[61]

In this study, a nanosecond, pulsed electron paramagnetic resonance (EPR) technique has been applied to characterize β for charge-recombination (CR) reactions in several intermolecular RIP systems produced by the triplet-precursor photoinduced ET reactions in fluid solutions. To determine β, the RPM electron spin polarization is quantitatively analyzed by numerical computations using the SLE[51−53] in which the following effects are included for the RIPs: (1) the spin exchange integral contribution to $2J$, (2) contributions of multiconfiguration interactions from several locally excited states involved in J_{CT}, and (3) the r-dependent Coulomb attraction potential contributing to the mutual translational diffusion motions and to the driving force ($-\Delta G_{CR}$) for the charge-recombination.

We present a simple three-dimensional model of multiple electron tunneling pathways through intervening solvent molecules to account for not only the present experimental results but also the previously reported β values[12,38−41,62,63] in condensed media.

II. Experimental Section

Pulsed EPR measurements were carried out using an X-band pulsed EPR spectrometer (Bruker ESP 380E) equipped with a dielectric resonator at a Q factor of about 100. The microwaves were amplified by a 1-kW traveling wave tube amplifier, and the pulse sequences were triggered by a synchronous output of an Nd−YAG laser (Qanta-Ray GCR-150, 30 Hz, ∼6 ns duration) as an excitation light source. A two-pulse ($\pi/2-\tau-\pi$) echo sequence with a CYCLOPS phase-cycling routine was employed to prevent the dead-time problem. τ was set to 88 ns. The echo signals were accumulated by a digital oscilloscope (LeCroy Model 9450A) synchronized with a microwave pulse programmer. A width of about 16 ns for the $\pi/2$ pulse was utilized in the present study. A temperature-control system (Bruker ER 4131 VT) was used to regulate the temperature. The resonator was inserted into a home-built dewar in which temperature-controlled gaseous nitrogen was used as a coolant. The microwave frequency was detected with a frequency counter (HP 5342A).

All solvents, *N*,*N*-dimethylformamide (DMF, Nacalai tesque), dimethyl sulfoxide (DMSO, Nacalai tesque), and benzonitrile (PhCN, Tokyo Kasei), were GR grade commercially available and were used as received. Duroquinone (DQ, Tokyo Kasei), 2,5-dimethyl-*p*-benzoqionone (XQ, Tokyo Kasei), chloro-*p*-benzoquinone (ClQ, Tokyo Kasei), 2,6-dichloro-*p*-benzoquinone (DClQ, Tokyo Kasei), 9,10-anthraquinone (AQ, Tokyo Kasei), and zinc tetraphenylporphyrin (ZnP, Aldrich) were recrystallized from methanol or ethanol. *N*,*N*-dimethyaniline (DMA, Tokyo Kasei) was distilled before use. GR-grade *N*,*N*,*N*′*N*′-tetramethylbenzidine (TMBD, Tokyo Kasei) was used as received. The sample solutions were deoxygenated by passages of Ar gas for 30 min and flowed through the quartz EPR tube (2.5 mm od). For the ZnP−quinone systems in PhCN, the sample solutions were deoxygenated by freeze−pump−thaw cycles using a vacuum line technique. For the ZnP−quinone systems, the excitation light source was the second harmonics (532 nm) of the Nd−YAG laser that selectively excited ZnP; otherwise, the third harmonic (355 nm) was used to excite selectively the quinone species.

The oxidation and reduction potentials of the reactant molecules were measured using a cyclic voltammeter (Model P-1000, YANACO) under deaerated conditions achieved by nitrogen bubbling. 0.1 M tetra-*n*-propylanmonium perchlorate (TPAP, Nacalai tesque) was used as the supporting electrolyte. Working and counter electrodes were platinum while the reference electrode was the standard calomel electrode (SCE). A gaseous nitrogen flow cryostat was used to control temperature of the sample solution. Details are described in the Supporting Information of ref 60.

III. Results and Discussion

A. Measurements of CIDEP Originating from Radical Ion Pairs. Figure 1 shows the temperature dependence of an echo-detected Fourier transformed (FT) EPR spectrum observed at a delay time of 200 ns for the $\pi/2$ microwave pulse after the 355-nm laser excitation of DQ (10 mM) in the presence of DMA (14 mM) in DMF solution. The EPR signals are assigned to the DQ anion radical ($DQ^{\bullet-}$) based on the reported g value

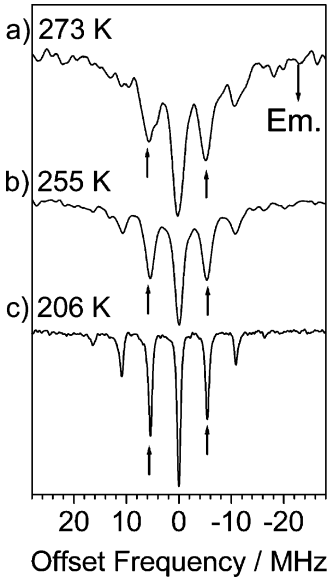

Figure 1. Temperature dependence of FT-EPR spectrum of the duroquinone anion radical observed at 200 ns after the laser excitation of DQ (10 mM) in the presence of DMA (14 mM) in DMF.

($g = 2.0049$) and hyperfine coupling constants.[64] Since the external magnetic field was set to the resonance frequency at $g = 2.0049$, Figure 1 displays the hyperfine structure of the center part of $DQ^{\bullet-}$. The photoinduced ET reaction predominantly takes place from the T_1 state of quinone because of fast (<6 ps) intersystem crossing of the S_1 state of quinone molecules.[65] The net microwave emissive (em) CIDEP is assigned to the triplet mechanism (TM),[50,66,67] reflecting the electron spin polarization of the precursor excited triplet state of the quinone molecules. At 273 K (a), the emissive signal intensity is smaller at the higher frequency of +5.5 MHz (defined here as $M_I = 1$) than that at −5.5 MHz ($M_I = -1$) as indicated by the arrows on the peaks. This is explained by the contribution of the hyperfine-dependent RPM polarization.[50,54] The phase of the RPM polarization is the absorption/emission (A/E) type, representing $J > 0$ at the effective RPM CIDEP generation distance.[47,60] At 206 K, the RPM phase is inverted to E/A-type polarization representing $J < 0$ in the RIP of $DMA^{\bullet+}\cdots DQ^{\bullet-}$. The inversion of the sign of the J has been reported for several donor−quinone systems in the previous studies and is explained in terms of the charge-transfer mechanism in the J.[59,60,68]

To evaluate the RPM polarization contributions, we examined the delay time dependences of the FT-EPR signal intensities. The external magnetic fields were set to the resonance peak positions at ±5.5 MHz shown by the arrows in Figure 1. We recorded dependences of the signal peak intensities on the delay time between the $\pi/2$ microwave and the laser pulses. Line widths of the signals of the quinone anion radicals were independent of the delay times in the present study. Figure 2 shows time profiles of the additions (filled circles) and subtractions (open circles) between the signal intensities at the offset frequencies of 5.5 and −5.5 MHz in Figure 1. The filled circles represent the net (hyperfine independent) polarized signal contribution, while the open circles represent the hyperfine-dependent RPM signal contribution. In the filled-circle plots, the negative value denotes microwave emission. Positive components around the several microsecond region represent the absorptive thermal equilibrium electron spin population (P_{eq}) after the spin−lattice relaxation of polarized $DQ^{\bullet-}$.[54] In the open-circle plots, a positive value denotes the A/E-type polarization, while a negative one denotes the E/A polarization. In Figure 2c, the signal rise of the filled circle is faster than the rise of the open circle. This is because the rise of the TM polarization is dominated by the spin−lattice relaxation rate ($1/T_{1T} = 10^8\ s^{-1}$) of excited triplet states in the liquid phase while the rise of the RPM components is governed by a bimolecular ET reaction rate of $10^7\ s^{-1}$.[54] In the filled-circle plots, the RPM may also contribute to the polarization via the effect of the Zeemann energy difference (Δg effect) in the RIP since the g value ($g = 2.0033$)[69] of the counter radical ($DMA^{\bullet+}$) is smaller than the g value of $DQ^{\bullet-}$. The subsequent slower rise in emissive signal (filled circles) in part c of Figure 2 clearly shows the Δg effect of the RPM polarization since the rise is consistent with the rise in the open circle. Evidently, from the open circles, the phase of the RPM magnetization is inverted from the A/E in part a to the E/A-type polarization in part c with decreasing temperature in Figure 2.

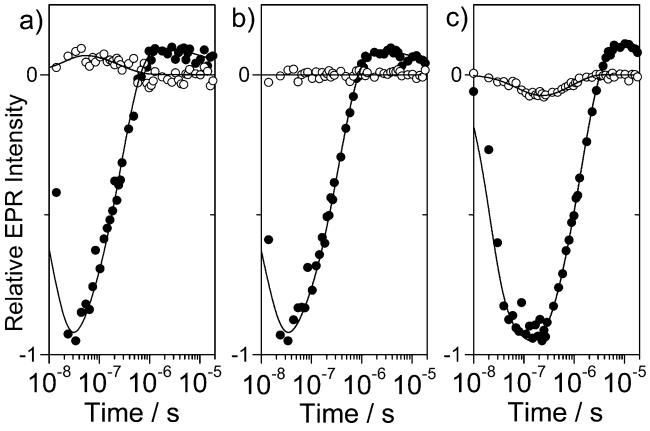

Figure 2. Delay-time dependence of the additions (●) and subtractions (○) of the signal intensities at the offset frequencies of 5.5 and −5.5 MHz at (a) 273 K, (b) 255 K, and (c) 206 K in Figure 1 for the photoinduced ET reaction system of $^3DQ + DMA \rightarrow DQ^{\bullet-} + DMA^{\bullet+}$ in DMF. Solid curves show simulations by eqs 3 and 4 using parameters listed in Table 1.

The thermal equilibrium spin population of P_{eq} is experimentally observed at several microseconds as shown in Figure 2, and the rise times of the TM and the RPM polarization can be distinguished from each other in the present pulsed EPR measurements. Therefore, we can separate the contributions of the TM and the RPM to determine the absolute magnitudes of the TM and the RPM polarization, respectively in units of P_{eq}. The time developments of the transient magnetization of M_Z on quinone anion radicals ($Q^{\bullet-}$) were computed as shown with the solid lines in Figure 2 by numerical analysis of the following differential equations[70−73] (see Supporting Information for the equation derivations)

$$\frac{dM_{Z,M_I}}{dt} = \frac{P_{eq}[Q^{\bullet-}] - M_{Z,M_I}}{T_1} + P_{TM}k_q[D]c_0 \exp\left\{-\left(k_q[D] + \frac{1}{T_{1T}}\right)t\right\} + \frac{4}{3}P_{eq}k_q[D]c_0\left[\exp(-k_q[D]t) - \exp\left\{-\left(k_q[D] + \frac{1}{T_{1T}}\right)t\right\}\right] + P_{RPM}(M_I)\{k_q[D]c_0 \exp(-k_q[D]t) + k_b[Q^{\bullet-}][D^{\bullet+}]\} \quad (3)$$

with

$$\frac{d[Q^{\bullet-}]}{dt} = k_q[D]c_0 \exp(-k_q[D]t) - k_b[Q^{\bullet-}][D^{\bullet+}] \quad (4)$$

TABLE 1: Redox Potentials and Global Fitting Parameters in eqs 3 and 4

solvent temp/K	donor $E^{ox}_{1/2}$/V	acceptor $E^{red}_{1/2}$/V	$-\Delta G_{CR0}$/eV[a]	$c_0k_b/10^4$ s^{-1}	k_q[D]/10^7 s^{-1}	T_1/μs	T_{1T}/ns	P_{TM}/P_{eq}	$P_{RPM}(M_I)/P_{eq}$[c] $M_I=-1$[b]	$P_{RPM}(M_I)/P_{eq}$[c] $M_I=+1$[b]	Q_{+1}/Gauss
DMF	DMA	DQ									
273	0.97	−0.75	1.72	5.0	7.5	0.28	6	−42	1.2	2.3	2.35
	DMA	DQ									
255	0.92	−0.71	1.63	5.0	6.0	0.35	6	−49	0.0	0.0	2.35
	DMA	DQ									
206	0.90	−0.69	1.59	1.0	1.2	1.4	10	−60	−3.2	−4.8	2.35
		DClQ									
		−0.15	0.80	2.5	3.8	1.0	35	80	−12	−22	3.60
		ClQ									
PhCN	ZnP	−0.32	0.97	9.0	4.5	0.62	20	100	−6.5	−12	2.75
273	0.65	XQ									
		−0.61	1.26	1.8	3.0	2.4	35	25	−4.0	−5.1	2.50
		DQ									
		−0.84	1.49	28	0.12	0.36	25	25	3.6	4.7	2.50
DMSO	TMBD	AQ									
295	0.50	−0.74	1.24	5.0	0.38	1.4	10	−150	−0.9	−1.6	1.44

[a] $-\Delta G_{CR0} = E^{ox}_{1/2} - E^{red}_{1/2}$. [b] $M_I = +1$ is defined as the nuclear spin quantum states of quinone anion radicals at the higher-frequency positions shown by the arrows on the hyperfine lines in Figures 1, 4, and 6a, while $M_I = -1$ denotes the nuclear states at the lower-frequency positions. [c] Resonance positions of the centers of the countercation radicals locate at higher fields than $M_I = -1$ line positions, leading to identical RPM phases for $M_I = -1$ and $M_I = +1$ positions.

In eq 3, T_1 and T_{1T} denote the spin−lattice relaxation times of $Q^{\bullet-}$ and the excited triplet states, respectively. P_{TM} and $P_{RPM}(M_I)$ (of the Ith hyperfine line) specify the TM and the RPM polarization magnitudes. k_q represents the forward ET reaction rate constant between the excited triplets and the D molecules. k_b represents the bimolecular back ET rate constant between the $Q^{\bullet-}$ and $D^{\bullet-}$ molecules. c_0 is the initial concentration of excited triplet state created by the laser excitation and by the intersystem crossing. The constant $c_0 \approx 10^{-5}$ M was estimated from the laser power and the irradiated volume of the sample. $[Q^{\bullet-}] = [D^{\bullet+}]$ is assumed in eqs 3 and 4. In eq 3, $(^4/_3)P_{eq}$ represents the thermal equilibrium spin population of the precursor triplet state, which contributes to the net absorptive CIDEP on the observed radicals.[74] The time developments of the computed quantities of $(M_{Z,1} + M_{Z,-1})$ and $(M_{Z,1} - M_{Z,-1})$ were convoluted with the response functions determined by the width (16 ns) of the $\pi/2$ microwave pulse.[48] Several time-resolved EPR studies have suggested that homogeneous ET reactions between quinone anions and the dissolved neutral quinone molecules affect the decay time of the multiplet $(M_{Z,1} - M_{Z,-1})$ contributions.[69,75,76] However, even if homogeneous ET were to occur, the effect needs not to be taken into account in this study, because both the net and the multiplet contributions were simulated with a common, single T_1 parameter in eq 3 as seen in Figure 2. These results indicate that the homogeneous ET rate is much slower than the original spin−lattice relaxation times of quinone anion radicals in the solvents used in this study.

The temperature effect on the oxidation and reduction potentials was measured for DMA and DQ,[59,60] respectively (see Supporting Information). In Table 1, the redox potentials and the driving forces defined by $-\Delta G_{CR0} = E^{ox}_{1/2} - E^{red}_{1/2}$ are shown together with the results of the global fitting parameters of Figure 2 using eqs 3 and 4. As was reported in the previous studies, the RPM polarization (P_{RPM}) gets inverted from a negative (showing $J < 0$) to a positive ($J > 0$) value with increasing $-\Delta G_{CR0}$.[59,60] In Figure 3, the experimental $P_{RPM}(M_I = +1)$ values in Table 1 are plotted with respect to $-\Delta G_{CR0}$ by the filled circles.

Figure 4 displays echo-detected FT-EPR spectra obtained with the 532-nm laser excitations of ZnP (0.5 mM) in the presence of (a) DClQ (5 mM), (b) ClQ (5 mM), and (c) DQ (10 mM) at

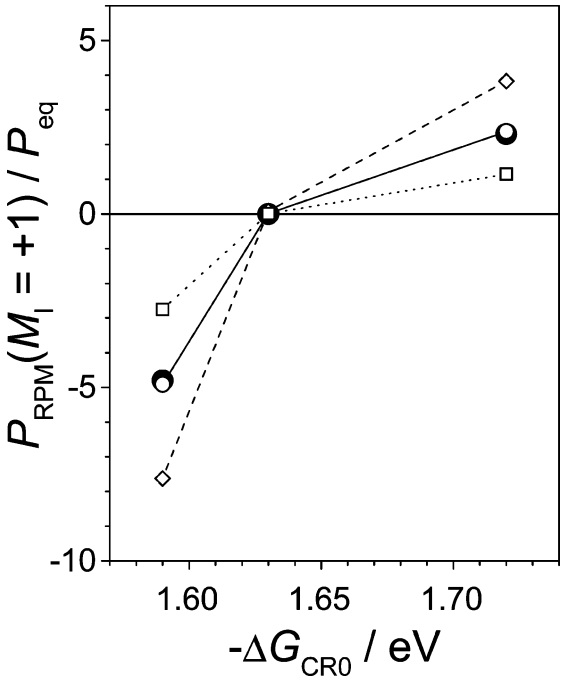

Figure 3. Driving-force ($-\Delta G_{CR0}$) dependence of RPM polarization (P_{RPM}) in the duroquinone anion radical at $M_I = +1$ obtained in the DMA−DQ system in DMF. Filled circles (Table 1) determined from Figure 2. Open circles connected with solid lines were calculated by finite-difference analysis of eqs A12−A27 under $\beta = 0.91$ Å^{-1} with $\gamma = 1.031$ in eq 15 and reproduce the entire experimental results. See text for details. Open squares and open diamonds were calculated under $\beta = 1.20$ Å^{-1} with $\gamma = 0.993$ and under $\beta = 0.80$ Å^{-1} with $\gamma = 1.049$, respectively.

273 K in a PhCN solution at the delay times of 0.1 μs in parts a and b and of 0.5 μs in part c. Sharp peaks in Figure 4 show hyperfine structures of (a) 2,5-dichloro-*p*-benzoqionone anion radical, (b) chloro-*p*-benzoqionone anion radical, and (c) $DQ^{\bullet-}$, respectively. In Figure 4, the external magnetic fields were set to the resonance positions at the g values of the corresponding quinine anion radicals, $g = 2.0052$ in (a), $g = 2.0050$ in (b), and $g = 2.0049$ in (c), respectively. Superimposed broad signals were assigned to ZnP cation radicals ($ZnP^{\bullet+}$) with $g = 2.0025$.[77] Since the deactivation rate (ca. 10^9 s^{-1}) of the first excited singlet

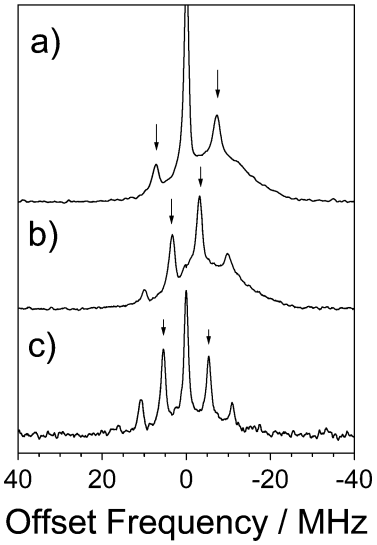

Figure 4. FT-EPR spectra obtained by the 532-nm laser excitations of ZnP (0.5 mM) in the presence of (a) DClQ (5 mM), (b) ClQ (5 mM), and (c) DQ (10 mM) at 273 K in PhCN at the delay times of 0.1 μs in parts a and b and of 0.5 μs in part c.

state of ZnP is much faster than the bimolecular reaction rate (k_q[D] $\approx 10^6-10^7$ s^{-1} as shown in Table 1) under the present quinone concentrations dissolved in PhCN, the photoinduced ET is dominated by the reactions from the excited triplet ZnP. The net absorptive polarization is interpreted by the TM contribution, reflecting absorptive electron spin polarization in ^{3}ZnP*.[77] In parts a and b in Figure 4, as indicated by arrows, signal intensities of the sharp peaks of quinone molecules are weaker at the higher frequency positions ($M_I = 1$) than the intensities at $M_I = -1$, denoting the E/A-type RPM CIDEP contribution. In part c, the signal intensity relationship between $M_I = 1$ and -1 indicates the A/E-type polarization. To obtain time profiles of the quinone signals, contributions of the CIDEP spectra of countercation radicals were subtracted by fitting polynomial functions to the broad baselines.[59] Figure 5 shows the time profiles of the additions (filled circles) and subtractions (open circles) between the signal intensities at the $M_I = 1$ and the $M_I = -1$ peaks in (a) ZnP-DClQ, (b) ZnP−ClQ, (c) ZnP-XQ, and (d) ZnP-DQ systems at 273 K in PhCN. Solid lines were simulated with the same procedures as mentioned above by using eqs 3 and 4. The oxidation and reduction potentials of ZnP and quinones were determined by the CV method as follows: $E^{ox}_{1/2}$(ZnP) = 0.65 V, $E^{red}_{1/2}$(DClQ) = −0.15 V, $E^{red}_{1/2}$(ClQ) = −0.32 V, $E^{red}_{1/2}$(XQ) = −0.61 V, and $E^{red}_{1/2}$(DQ) = −0.84 V. In Table 1, the redox potentials and the global fitting parameters are listed.

Figure 6a shows the center part ($g = 2.0044$) of a pulsed EPR spectrum of 9,10-anthraquinone anion radical produced by the 355-nm laser excitations of AQ (0.5 mM) in the presence of TMBD (1 mM) in DMSO at 295 K. The time profiles in Figure 6b were taken as the addition and the subtraction of the signal intensities at the higher and the lower frequency hyperfine lines indicated by arrows in Figure 6a. The strong net emissive CIDEP is assigned to the TM polarization of the excited triplet AQ because of the fast rise time (10 ns) in the filled circle plots; the signal rise is consistent with spin−lattice relaxation times of the excited triplet states in liquid phases. From the open circles in Figure 6b, a weak E/A-type polarization is observed on the anion radical. The solid lines in Figure 6b show simulations of the time profiles by using eqs 3 and 4. The fitting parameters are listed in Table 1 together with the oxidation and

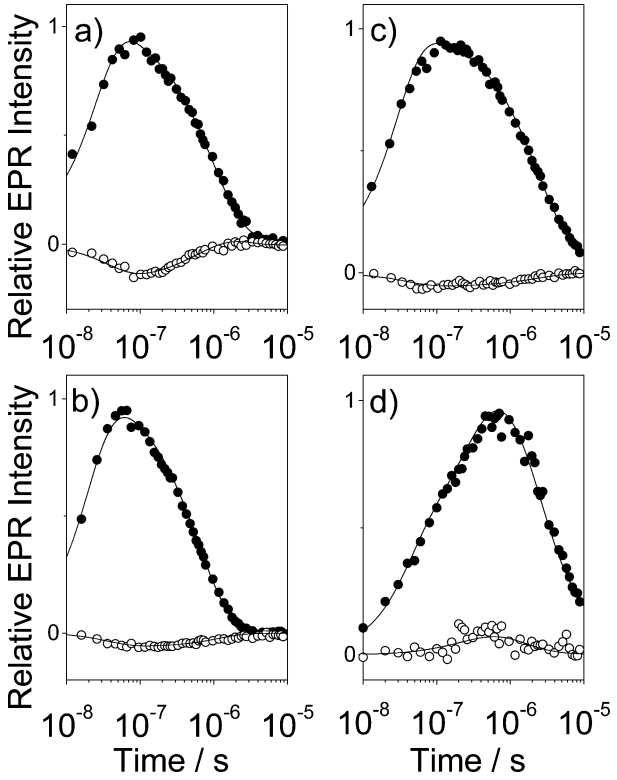

Figure 5. Delay-time dependence of the additions (●) and subtractions (○) of the signal intensities between $M_I = 1$ and -1 signals on quinone anion radicals obtained in (a) ZnP−DClQ, (b) ZnP−ClQ, (c) ZnP−XQ, and (d) ZnP−DQ systems in PhCN at 273 K. Solid curves show simulations by eqs 3 and 4. Fitting parameters are listed in Table 1.

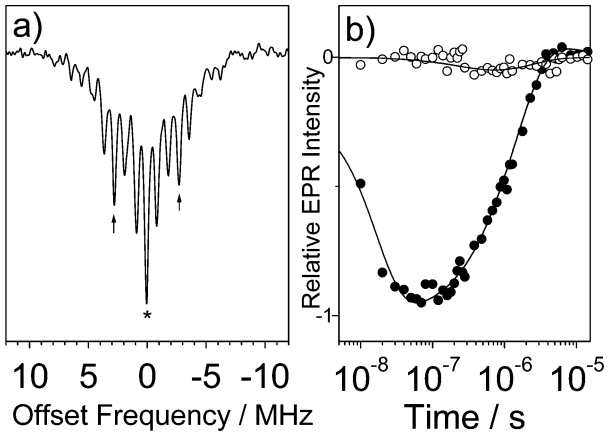

Figure 6. (a) Center part of the pulsed EPR spectrum of the 9,10-anthraquinone anion radical observed by the 355-nm laser excitation of TMBD−AQ (1 mM, 0.5 mM) system in DMSO at room temperature. (b) Time profiles of the additions (●) and subtractions (○) of the signal intensities at the peaks indicated by arrows in part a.

reduction potentials of TMBD and AQ measured in DMSO solution at room temperature. P_{RPM} values were obtained for the individual solvent-separated RIP systems under the several conditions, as listed in Table 1.

In all D−A systems in Table 1, since the relation of k_q[D] < $1/T_{1T}$ is satisfied, we are able to separately examine the TM and the RPM contributions by the analysis of the pulsed EPR data using eqs 3 and 4. In DMA−DQ systems, k_q values were obtained to be $k_q = 5.4 \times 10^9$, 4.3×10^9, and 8.6×10^8 M^{-1} s^{-1}, which are quite consistent with the diffusion limit under the viscosities of 1.2 cP (at 273 K), 1.6 cP (at 255 K), and 4.1 cP (at 206 K) in DMF. These k_q values are consistent with the

bimolecular ET reaction rate constants, because the free energy change ($\Delta G_{CS} = E^{ox} - E^{red} - E_T^{DQ}$) is negative ($\Delta G_{CS} \approx -0.8$ eV) for the forward ET from the excited triplet state ($E_T^{DQ} = 2.39$ eV[78]) of DQ. For the other systems, k_q values were also consistent with the diffusion-controlled rate constants if the free energy relationship is feasible for the triplet precursor ET reactions $\Delta G_{CS} < -0.2$ eV. In the ZnP−DQ system, $k_q = 1.2 \times 10^8$ M^{-1} s^{-1} obtained is about 30 times smaller than the diffusion limit in PhCN (1.9 cP at 273 K). This is explained by the fact that the free energy (1.49 eV) of the CS state is almost comparable to the excited triplet state energy ($E_T^{ZnP} = 1.53$ eV)[78] of ZnP, i.e., $\Delta G_{CS} \approx 0$ eV. These results show that the k_q values are valid as the bimolecular ET reaction rate constants and strongly support the validity of the P_{RPM} values determined in Table 1.

B. Computation of Singlet−Triplet Energy Splitting (2*J*) in Radical Ion Pairs. Generally, the singlet−triplet energy gap (or exchange interaction 2*J*) is composed of (1) a two-electron exchange integral (J_{EX}) and (2) a charge-transfer interaction (J_{CT}) as follows[43,79]

$$2J(r) = J_{EX}(r) + J_{CT}(r) \tag{5}$$

In randomly oriented molecular systems, J_{EX} is dominated by the exchange integral described as[43,79]

$$J_{EX} = -\left\langle \varphi_{D^+}(1)\varphi_{A^-}(2)\left|\frac{e^2}{4\pi\epsilon_0 r_{12}}\right|\varphi_{D^+}(2)\varphi_{A^-}(1)\right\rangle \tag{6}$$

where φ_j represents a singly occupied MO of the radical cation ($D^{\bullet+}$) and radical anion ($A^{\bullet-}$) for unpaired electrons 1 and 2 separated by a distance r_{12}. e is the charge on an electron, and ϵ_0 is the permittivity of vacuum. In randomly oriented radical pairs, J_{EX} is usually expressed with an exponentially decaying function with respect to r, as $J_{EX}(r) = J_0 \exp[-\alpha(r - d)]$. In this study, $J_0 = 10^{12}$ rad/s at $d = 6$ Å and $\alpha = 2$ $Å^{-1}$ is adopted from a recent quantitative CIDEP study of the RPM polarization analysis of a neutral radical pair composed of the hydroxymethylethyl radical.[80]

The charge-transfer interaction J_{CT} has been formulated as the configuration interaction using second-order perturbation theory induced by the electronic coupling (or transfer integral) of V_{DA} between the RIP state (*e*) and the charge-recombined states (*G*), including the molecular vibrational quantum effects as follows[47,61]

$$J_{CT}(r) = \sum_G \sum_j \int_{-\infty}^{\infty} \frac{(1 - 2S_G)V_{DA}(r)^2 \prod_b \mathrm{FC}_G(j_b)}{E_e(X,r,\mathbf{i}=\mathbf{0}) - E_G(X,r,\mathbf{j})} P_e(X,r)\, dX \tag{7}$$

where **j** represents a set of intramolecular vibration quantum numbers j_b for several modes *b*; $\mathbf{j} = (j_1, j_2, ..., j_b, ...)$ in the *G* state. $\mathbf{i} = \mathbf{0}$ means that only the zero-point vibrational levels can be populated in the *e* state when the high-frequency modes are taken into account for the intramolecular reorganizations. In eq 7, S_G is the electron spin quantum number of the *G* states; $S_G = 0$ for singlet and $S_G = 1$ for triplet states. P_e denotes the probability that the *e* state is populated with respect to the normalized solvent coordinate (X).[47] E_e and E_G represent potential-energy surfaces of the *e* and the *G* states, respectively. According to Marcus theory, the solvent−solute interaction potential-energy surfaces can be considered to be parabolic with respect to X. E_e and E_G are then expressed as follows

$$E_e(X,r,\mathbf{i}=\mathbf{0}) = \lambda_S(r)X^2 - \Delta G_{CR}(r) \tag{8}$$

$$E_G(X,r,\mathbf{j}) = \lambda_S(r)(X-1)^2 + \sum_b j_b h\upsilon_b + E_G \tag{9}$$

where $\lambda_S(r)$ denotes the solvent reorganization energy. υ_b is the vibrational frequency of the mode *b*. E_G is the zero-point free energy of the *G* electronic states. $-\Delta G_{CR}$, as the zero-point free energy of the *e* state, is obtained by using the half-wave oxidation ($E^{ox}{}_{1/2}$) and reduction ($E^{red}{}_{1/2}$) potentials for the D and A molecules, respectively, as

$$-\Delta G_{CR}(r) = E_{1/2}{}^{ox} - E_{1/2}{}^{red} - \frac{e^2}{4\pi\epsilon_0\epsilon_S r} \tag{10}$$

where the last term denotes the Coulomb attraction potential within the RIP and ϵ_S denotes the static dielectric constant of solvent. In eq 7, FC represents the Franck−Condon factor between the *e* and *G* state intramolecular vibrations described as[47]

$$\mathrm{FC}_G(j_b) = \exp(-\sigma_G)\frac{\sigma_G{}^{j_b}}{j_b!} \tag{11}$$

$$\sigma_G = \frac{\lambda_{V,G}}{h\upsilon_b} \tag{12}$$

where $\lambda_{V,G}$ is the intramolecular reorganization energy in the state of *G*. In eq 7, P_e is represented as

$$P_e(X,r) = \left(\frac{\lambda_S(r)}{2\pi k_B T}\right)^{1/2} \exp\left\{-\frac{\lambda_S(r)}{2k_B T}X^2\right\} \tag{13}$$

The *r*-dependent solvent reorganization energy $\lambda_S(r)$ is represented by the well-known continuum dielectric model[10]

$$\lambda_S(r) = \frac{e^2}{4\pi\epsilon_0}\left(\frac{1}{2d_D} + \frac{1}{2d_A} - \frac{1}{r}\right)\left(\frac{1}{n_D{}^2} - \frac{1}{\epsilon_S}\right) \tag{14}$$

where d_D and d_A denote the effective solvation radii of the D and A molecules. n_D denotes the refractive index. Applicability of the continuum model of eq 14 has been discussed for several ET reaction systems at long-range D−A distances.[59,60,68,81−83] In the intramolecular ET systems, failure of the continuum model was observed in the temperature dependence of the λ_S at relatively short D−A distances of 3 and 6 Å.[81,84] Origin of the failure has been identified as the density fluctuations and associated translational motions of the solvent molecules around the solutes during the intramolecular ET processes.[81] These fluctuating motions were however predicted by Vath et al. to be negligible for rather separated redox pairs and the intermolecular ET systems.[81] In our previous studies, the solvent polarity (n_D and ϵ_S) effect on λ_S was explained by eq 14 for the 1,2,4-trimethoxybenzene cation and the duroquinone anion solvent-separated RIP system in DMF and butyronitrile.[60] In the present study, calculated molecular radii (a_D and a_A) of the solute molecules were determined by the solute volumes (V_S) using the relationship of $a = (3V_S/4\pi)^{1/3}$, where the molecular volumes were calculated with the density functional theory (DFT) method (UB3LYP/6-31G* volume) using the Gaussian 98 suites of

TABLE 2: Solvent and Solute Parameters, Calculated RPM Polarization (P_{+1}^{calc}), and Distance Dependence (β) of Electronic Coupling Obtained by the Finite-Difference Analysis[a]

solvent T/K	donor	acceptor	a_D/Å	a_A/Å	n_D^2	ϵ_s	$\lambda_{V,D}$/eV	$\lambda_{V,A}$/eV	$D/10^{-6}$ cm^2 s^{-1}	β/Å^{-1} [b]	P_{+1}^{calc}/P_{eq}
DMF											
273	DMA	DQ	3.47	3.58	2.08	42.1	0.09	0.25	9.49	0.91	2.4
255	DMA	DQ	3.47	3.58	2.10	45.9	0.09	0.25	6.79	0.91	0.0
206	DMA	DQ	3.47	3.58	2.17	58.3	0.09	0.25	2.10	0.91	−4.9
	ZnP	DClQ	6.02	3.42	2.37	28.8	0.42	0.28	4.73	0.87	4.8
PhCN	ZnP	ClQ	6.02	3.36	2.37	28.8	0.42	0.27	4.78	0.97	−5.2
273	ZnP	XQ	6.02	3.30	2.37	28.8	0.42	0.26	4.84	0.96	−12
	ZnP	DQ	6.02	3.58	2.37	28.8	0.42	0.25	4.67	0.88	−21
DMSO											
295	TMBD	AQ	4.24	3.97	2.18	46.7	0.18	0.16	4.06	1.01	−1.5
DMF											
258	TMB	DQ	3.69	3.58	2.10	44.9	0.31	0.25	6.98	0.83	0.0

[a] $\gamma = 1.031$ is set in eq 15. [b] β to fit the experimental $P_{RPM}(M_I = +1)$ values in Table 1.

program.[59,60] In Table 2, the calculated molecular radii of a_D and a_A are listed for the donor and acceptor molecules, respectively. The effective, experimentally determined molecular sizes (d_D and d_A) are defined as follows

$$d_D = \gamma a_D \quad d_A = \gamma a_A \tag{15}$$

Here, γ is treated as one of the fitting parameters for reproducing the values of P_{RPM} in the DMA−DQ systems. In all cases, γ is close to unity as expected when this approach is valid. The parameters n_D and ϵ_S were obtained from the following relations:[85] $dn_D/dT = -5.0 \times 10^{-4}$ K^{-1}, $d(\ln \epsilon_S)/dT = -4.9 \times 10^{-3}$ K^{-1} for DMF, $dn_D/dT = -5.8 \times 10^{-4}$ K^{-1}, and $d(\ln \epsilon_S)/dT = -3.2 \times 10^{-3}$ K^{-1} for PhCN. These relationships were obtained from the reported values of n_D and ϵ_S at several temperatures.[86−88] For DMSO, $n_D = 1.4771$ and $\epsilon_S = 46.7$ are reported at room temperature.[78] The dielectric parameters are listed in Table 2.

For J_{CT} computations in eq 7, a total of five charge-recombined configurations were taken into account as the G states: a ground-state donor−acceptor pair of $D(S_0)\cdots A(S_0)$, two locally excited triplet states of $^*D(T_1)\cdots A(S_0)$ and $D(S_0)\cdots {}^*A(T_1)$, and two locally excited singlet states of $^*D(S_1)\cdots A(S_0)$ and $D(S_0)\cdots {}^*A(S_1)$. The configuration interactions from the upper excited states (T_2, S_2, and so on) are negligible in the present study because these energy levels are expected to be much higher than the energies of $-\Delta G_{CR0}$. The configuration interaction from doubly charged-state pairs of $^{1,3}(D^{2+}\cdots A^{2-})$ was also ignored.[48] $E_G = 0.00$ eV is set when $G = D(S_0)\cdots A(S_0)$ in eq 9. The free energies of excited states were utilized as follows: E_{T1}(DQ) = 2.39 eV,[78] E_{S1}(DQ) = 2.58 eV,[89] E_{T1}(DMA) = 3.29 eV,[78] E_{S1}(DMA) = 4.10 eV,[90] E_{T1}(DClQ) = 2.38 eV,[78] E_{S1}(DClQ) = 2.58 eV, E_{T1}(ClQ) = 2.38 eV, E_{S1}(ClQ) = 2.58 eV, E_{T1}(XQ) = 2.30 eV,[91] E_{S1}(XQ) = 2.58 eV, E_{T1}(ZnP) = 1.53 eV,[78] E_{S1}(ZnP) = 2.08 eV,[78] E_{T1}(TMBD) = 2.73 eV,[92] E_{S1}(TMBD) = 3.73 eV,[92] E_{T1}(AQ) = 2.71 eV,[78] E_{S1}(AQ) = 2.90 eV,[78] E_{T1}(1,2,4-trimethoxybenzene, TMB) = 3.3 eV, and E_{S1}(TMB) = 4.32 eV.[90] Since the free energies of the excited singlet and triplet states are much higher than the $-\Delta G_{CR0}$ energies in the present study, the configuration interactions from the excited states play minor roles in the J_{CT} calculations except for the ZnP−DQ system, in which E_{T1}(ZnP) = 1.53 eV is quite close to $-\Delta G_{CR0} = 1.49$ eV.

In eq 2, V_0 and β were assumed to be independent of the G state. V_0 was fixed to 1100 cm^{-1} at 3.5-Å separation. This V_0 value was determined for the ET processes of the charge-transfer complex between several electron donors and an acceptor of dicyanodichlorobenzoquinone.[93] In the present study, the closest distance was set to be $d = 6$ Å; therefore, $V(d) = 1100 \exp\{-\beta(6 - 3.5)\}$ cm^{-1} was obtained. $V(d = 6$ Å) amounts to about 300−350 cm^{-1} when $\beta = 0.9$−1.0 Å^{-1} is utilized. This value is consistent with the experimentally obtained electronic coupling matrix element for intermolecular ET reactions at $d = 6$−7 Å in both liquid and frozen solutions.[40,62,94] β was treated as another fitting parameter to reproduce the values of P_{RPM} in Table 1.

For the intramolecular reorganizations, we considered a single, high-frequency vibration mode of $\upsilon_b = 1500$ cm^{-1} (as C═O, C−N, or C−O stretching). Geometry optimizations of the ion radicals and neutral ground states were performed with the UB3LYP DFT calculations with the 6-31G* basis set. At the optimized nuclear geometries for the ion radicals, energies for neutral species were obtained by single-point energy calculations. The molecular λ_V values ($\lambda_{V,D}$ and $\lambda_{V,A}$) are defined as the energy differences between the two geometries in the neutral electronic states of the D and A molecules, respectively[60] (Table 2). The validities of λ_V obtained by the UB3LYP/6-31G* level calculation were confirmed quantitatively.[95,96] In ZnP, $\lambda_{V,ZnP} = 0.42$ eV was adopted from the energy difference between vertical and adiabatic ionization potentials reported in the gas phase.[97,98] For $G = D(S_0)\cdots A(S_0)$, $\lambda_{V,G} = \lambda_{V,D} + \lambda_{V,A}$ was utilized for the computations of the Franck−Condon factor in eqs 11 and 12. For $G = {}^*D(T_1)\cdots A(S_0)$ and $G = {}^*D(S_1)\cdots A(S_0)$, $\lambda_{V,G} = \lambda_{V,A}$ can be set under the assumption that the solute structural changes are negligibly small between the radical cation of $D^{+\bullet}$ and the excited states of $^{1,3}D^*$. Similarly, for $G = D(S_0)\cdots {}^*A(T_1)$ and $G = D(S_0)\cdots {}^*A(S_1)$, $\lambda_{V,G} = \lambda_{V,D}$ was considered.

$J_{CT}(r)$ of eq 7 can be calculated for several D−A molecular systems by numerical integration with respect to X, using the parameters of the electronic coupling matrix element, excited-state energies described above, redox potentials in Table 1, molecular radii, solvent dielectric parameters, and intermolecular reorganization energies in Table 2. Figure 7 shows an example of the $-\Delta G_{CR0}$ dependence of $2J(r)$ calculated by eqs 5−15. This potential is computed for the $ZnP^{\bullet+}\cdots Q^{\bullet-}$ systems in PhCN at 273 K for $\beta = 0.9$ Å^{-1} with $d_D = 6.2$ Å, $d_A = 3.7$ Å, E_T(quinone) = 2.39 eV, E_S(quinone) = 2.58 eV, $\lambda_{V,D} = 0.42$ eV, and $\lambda_{V,A} = 0.25$ eV. It is noticeable from Figure 7 that the contribution of the $J_{EX}(r)$ is negligibly small in comparison to $J_{CT}(r)$ when we employ the parameters of $V(d)$ and β, both of which have been *experimentally determined* in the intermolecular ET systems.[11,40,93,99]

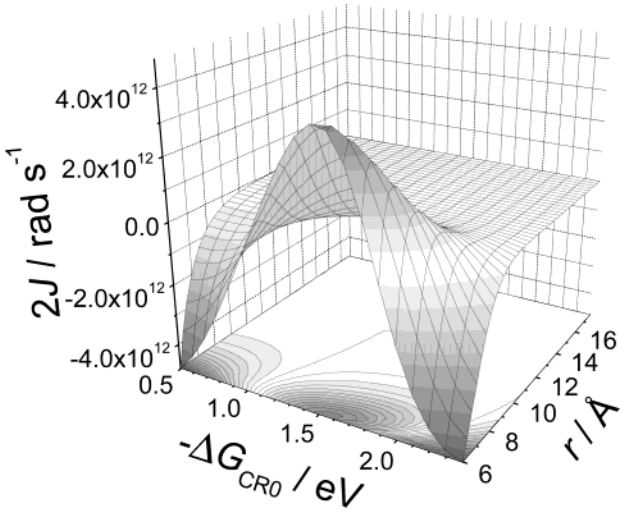

Figure 7. Driving-force ($-\Delta G_{CR0}$) dependence of $2J(r)$ calculated by eq 5 for the systems of ZnP cation and quinone anion RIPs in PhCN at 273 K with $\beta = 0.9$ Å^{-1}. $d_D = 6.2$ Å, $d_A = 3.7$ Å, E_{T1}(ZnP) = 1.53 eV, E_{S1}(ZnP) = 2.08 eV, E_{T1}(quinone) = 2.39 eV, E_{S1}(quinone) = 2.58 eV, $\lambda_{V,D} = 0.42$ eV, and $\lambda_{V,A} = 0.25$ eV were utilized. This result gives the solid line in Figure 8. A contour plot is shown on the bottom.

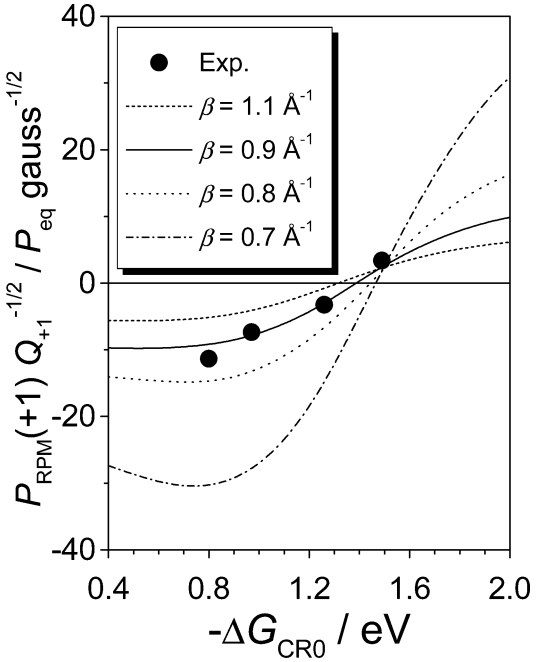

Figure 8. $-\Delta G_{CR0}$ dependence of $P_{RPM}(M_I = +1)/Q_{+1}^{1/2}$ in the ZnP−quinone systems (●) obtained from Table 1. Lines are calculated by the finite-difference analysis of eqs A12−A27 at different β values with $D = 4.8 \times 10^{-6}$ cm^2/s and $Q_{+1} = 2.5$ Gauss using the parameters in Figure 7.

On the basis of the $2J$ values computed as in Figure 7, the RPM polarization is calculated using the finite-difference analysis of the SLE, in which mutual radical diffusion motion is taken into account for the CIDEP generation, as reported in the previous study.[59] In this study, we considered the r-dependent Coulomb attraction potential affecting the mutual translational diffusions as adequate to discuss the β values for the solvent-separated RIPs. Details are described in the Appendix.

C. SLE Analysis of the Temperature Dependence of RPM CIDEP. First, we applied the finite-difference numerical analysis of the RPM polarization of eq A27 to reproduce the temperature dependence of $P_{RPM}(M_I = 1)$ in the system of DMA−DQ in DMF (Figure 3). For the computations in Figure 3, the variable fitting parameters of γ and β were assumed to be independent of temperature or $-\Delta G_{CR0}$. According to the solvent-mediated superexchange model in eq 18 (which will be discussed in section E), this assumption of the constant β value is applicable if the energy difference (ΔG_{DB}) of the oxidation potentials between the solvent and donor molecules and the difference (ΔG_{AB}) of the reduction potentials between the acceptor and solvent molecules are temperature independent. The solvent oxidation and reduction potentials may also be changed by temperature in accordance with the potential changes in the solute molecules, resulting in temperature-independent ΔG_{DB} and ΔG_{AB}. Under any given β parameter, the condition of $P_{RPM} = 0$ can be reproduced by varying the γ parameter; for example, in the case of $\beta = 1.2$ Å^{-1}, $P_{RPM}/P_{eq} = 0.0$ was obtained when $\gamma = 0.993$ is set in the numerical analysis. However, the absolute magnitudes of the polarization (plotted by the open squares in Figure 3) were calculated to be about two times smaller than the experimental $P_{RPM}(M_I = +1)$ values (plotted by the filled circles) at both 206 and 273 K, while the calculated magnitudes (plotted by the open diamonds) are larger than the experiments when $\beta = 0.8$ Å^{-1} is utilized. The RPM polarization magnitude will become large with a decrease in β because the effective polarization generation region or volume gets larger due to (1) the longer r_{eff} separation and (2) to the more gradual decay in the J interaction with respect to r; the effective re-encounter possibility around the r_{eff} separation becomes higher with the decrease in β.[61] This is quite compatible with the reported exponential dependence of the exchange interaction on the RPM polarization.[51] The best-fit calculation results were obtained when $\beta = 0.91$ Å^{-1} with $\gamma = 1.031$ were utilized, as shown by open circles in Figure 3. From eqs 14 and 15, $\gamma = 1.031$ indicates that the effective solute molecular sizes are larger by about 3% than the sizes estimated by the MO calculations, indicating that the Marcus continuum dielectric model is a good approximation for the solvent-reorganization energy in the liquid phase at long-range distance of r. This result is consistent with a recent theoretical analysis presented by Sato et al.[83] on a solvent reorganization energy calculation for the ionization process of DMA in acetonitrile using the ab initio reference interaction site model self-consistent field (RISM-SCF) theory. In the following analyses, $\gamma = 1.031$ is set for all solute molecules in the simulations of $P_{RPM}(M_I = +1)$ while evaluating the β values.[100]

D. Determinations of β for Solvent-Separated RIPs. According to the conventional re-encounter model theory of the RPM, P_{RPM} is proportional to the square-root of Q in eq.(A14).[50,55−58] Therefore, quantity of $P_{RPM}/Q^{1/2}$ is a rough indication of the efficiency of the RPM generation as normalized by Q. In Figure 8, $P_{RPM}(M_I = +1)/Q_{+1}^{1/2}$ values are plotted with respect to $-\Delta G_{CR0}$ for the ZnP−DClQ, ZnP−ClQ, ZnP−XQ, and ZnP−DQ systems from Table 1. Computations of the $-\Delta G_{CR0}$ dependence of $P_{RPM}/Q^{1/2}$ were performed for several β values as shown in Figure 8. The finite-difference analyses were performed using $2J(r)$ as shown in Figure 7, $D = 4.8 \times 10^{-6}$ cm^2/s, and $Q = 2.5$ Gauss. In Figure 8, it is obvious that the magnitude of the electron-spin polarization is quite sensitive to the β value. Experimental results of the filled-circle plots are mostly coincident with the calculated curve with a $\beta = 0.9$ Å^{-1}. This result clearly supports not only the validity of the mechanism of the J described above but also the applicability of the RPM CIDEP to characterize β values for several solvent-separated RIP systems.

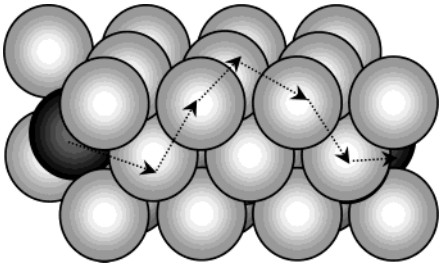

Figure 9. 3D pathway model of solvent-mediated superexchange coupling for intermolecular ET (between dark balls) separated by five intervening solvent molecules in condensed phase. One of the closest tunneling pathways is indicated by the arrows through nearest-neighbor solvent molecules separated by d_{SS}.

The β parameters were individually obtained by reproducing the several $P_{RPM}(M_I = +1)$ values in Table 1. Resultant β values are listed in Table 2 together with the calculated P_{RPM} values (P_{+1}^{calc}) by the finite-difference analyses using the parameters in Tables 1 and 2. In the previous study, $P_{RPM} = 0$ was obtained for the TMB−DQ system in DMF at 258 K by observing the temperature dependence of the RPM phase in $DQ^{\bullet-}$.[60] We also reproduced the $P_{RPM} = 0$ condition using the finite-difference analysis and determined β value as shown in Table 2.

E. Three-Dimensional Model of Superexchange Electronic Coupling in Intermolecular Electron Transfer. The McConnel superexchange mechanism[15] is a well-known means to account for the electronic-coupling matrix elements or β in several long-range ET reaction systems. Miller[12] first applied the model to the intermolecular ET as the superexchange through oxidized or reduced states of mediating solvents (B) to explain $\beta = 1.16$ Å^{-1} of $pyrene^{\bullet+}$ + TMPD → pyrene + $TMPD^{\bullet+}$ in a 2-chlorobutane glass matrix at 77 K. In the model, N numbers of equivalent *mediating* molecules were placed in one dimension (1D) between the donor and the acceptor molecules, as D B_1 $B_2 \cdots B_N$ A.[12] Here, we treat that model as a "1D model". The 1D model has been used to analyze the long-range ET reactions of hole and ETs in the Watson−Crick duplex of DNA.[21−28,31] However, in the intermolecular reaction systems in the condensed media, there will be a great deal of solvent molecules surrounding around the solute molecules. In protein ET reactions, electron tunneling was considered in terms of superexchange via multiple pathways through all valence orbitals of the protein.[36] In the intermolecular ET systems, we can also expect a large number of the solvent molecules to participate in the superexchange coupling for the long-range ET. We propose a simple model of 3D superexchange ET, in which the solvent molecules are assumed to be placed in close-packed, face-center cubic cells, as shown in Figure 9. When the donor and acceptor molecules are placed at the centers of the faces separated by 1, 3, and 5 intervening solvent molecules (see Figure 9), one can count 4, 36, and 384 *equivalent* nearest-neighbor superexchange routes, respectively, through the closest pathways between the solute molecules, ignoring the conformational differences in the solvent molecules. One of the closest routes separated by five intervening solvent molecules is shown by the arrows in Figure 9. This means that the solvent-mediated tunneling probability will become substantially greater in the 3D model than in the 1D model. The number (M) of mean, equivalent pathways is expected to grow exponentially with an increase in the number (N) of the intervening solvent molecules between D and A. Figure 10 shows a plot of M obtained at each number of N. From these plots, M may be approximated with $M = \exp(1.19N)$ as indicated by a solid line in Figure 10.

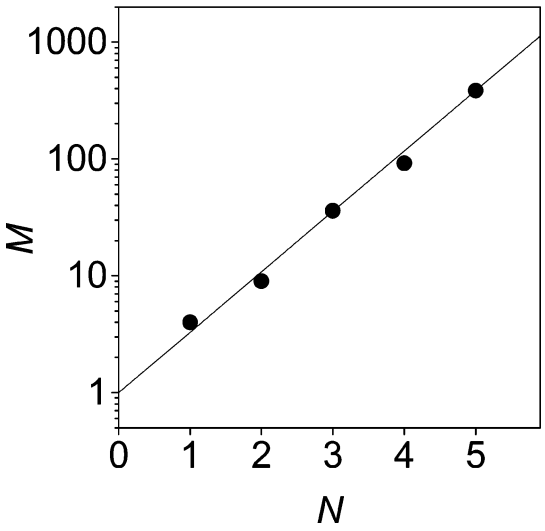

Figure 10. Semilog plot of equivalent closest nearest-neighbor superexchange pathways (M) with respect to the number (N) of the intervening solvent molecules obtained from the 3D model in Figure 9. The solid line represents a best fitting result of the exponential function of $M = \exp(1.19N)$.

The superexchange electronic coupling is described as follows[27,28]

$$V_{DA} = \sum_{route} \left\{ \frac{v_+(D,B_1)v_+(B_N,A)}{\Delta G_{DB1} + \lambda_1^{D}/2} \prod_{j=1}^{N-1} \frac{v_+(B_j,B_{j+1})}{\Delta G_{DB_{j+1}} + \lambda_{j+1}^{D}/2} + \frac{v_-(D,B_1)v_-(B_N,A)}{\Delta G_{AB1} + \lambda_1^{A}/2} \prod_{j=1}^{N-1} \frac{v_-(B_j,B_{j+1})}{\Delta G_{AB_{j+1}} + \lambda_{j+1}^{A}/2} \right\} \quad (16)$$

where v_+ and v_- denote electronic coupling between the adjacent molecules for hole and electron-transfer reactions, respectively. ΔG_{DB} and ΔG_{AB} represent adiabatic energy gaps for the hole and electron transfers from the solutes to the solvent molecules, respectively. λ_j represents total (solvent plus inner-sphere) reorganization energy and plays a role of offsetting the effective energy gaps from the adiabatic energy gaps, as reported by Tong et al.[27] The electronic couplings between the adjacent molecules are approximated to be the same as the solvent−solvent electronic coupling. ($v_+ = v_- = v_B$) Then, the 3D-model electronic coupling is represented from Figure 10 as follows

$$V_{DA}^{(3D)} = e^{1.19N} v_B^{N+1} \left\{ \left(\Delta G_{DB} + \frac{\lambda}{2} \right)^{-N} + \left(\Delta G_{AB} + \frac{\lambda}{2} \right)^{-N} \right\} \quad (17)$$

From eqs 2 and 17, the limiting formula of β is represented under $N \rightarrow \infty$, as follows

$$\beta^{(3D)} = \frac{2(2)^{1/2}}{d_{SS}} \ln\left(\frac{2\Delta G_{eff} + \lambda}{6.57 v_B} \right) \quad (18)$$

with

$$\Delta G_{eff} = \min(\Delta G_{DB}, \Delta G_{AB}) \quad (19)$$

For convenience the limiting form of the "straight-line" 1D model electronic coupling is expressed as follows[12]

$$\beta^{(1D)} = \frac{2}{d_{SS}} \ln\left(\frac{2\Delta G_{eff} + \lambda}{2 v_B} \right) \quad (20)$$

TABLE 3: Mean Solvent−Solvent Distances in the Liquid Solutions Estimated from eq 21 at Room Temperature

solvent	d_{SS}/Å
DMF	5.7 (5.7)[a]
PhCN	6.2
DMSO	5.5 (5.6)[b]
ethyleneglycol	5.1
C_2H_5OH	5.2
MTHF	6.2
2-chlorobutane	6.3
water	2.8[c]

[a] Estimated by Monte Carlo simulation.[101] [b] Determined by X-ray diffraction experiment.[102] [c] Oxygen−oxygen distance of amorphous ice at 77 K determined by Raman spectroscopy.[104]

In eqs 18 and 20, d_{SS} is defined as a mean center-to-center distance between the nearest-neighbor solvent molecules in the bulk, condensed media. Therefore, d_{SS} is estimated from solvent density (ρ_S) and from the solvent molecular weight (M_w) as follows

$$d_{SS} = \left(\frac{(2)^{1/2} M_w}{N_A \rho_S}\right)^{1/3} \quad (21)$$

where N_A is the Avogadro's number. As examples, from ρ_S(DMF) = 0.95 g/cm^3 and from ρ_S(DMSO) = 1.1 g/cm^3, d_{SS}(DMF) = 5.7 Å and d_{SS}(DMSO) = 5.5 Å are estimated at room temperature, respectively. The d_{SS}(DMF) value is consistent with the nearest intermolecular center-to-center distance (nitrogen−nitrogen = 5.7 Å) in the radial distribution function obtained by the Monte Carlo simulation of liquid DMF.[101] Also, the d_{SS}(DMSO) value is quite consistent with the first intermolecular peak (at 5.6 Å) observed in the radial distribution function obtained by the X-ray diffraction experiments of the pure liquid DMSO.[102] These results support the validity of eq 21 in predicting d_{SS}. Table 3 summarizes the mean values of solvent−solvent distances estimated from eq 21 for several liquid solutions at room temperature.

For several intermolecular ET reactions of the RIPs and of the reported reactant systems,[12,38−41] ΔG_{DB} and ΔG_{AB} can be obtained from oxidation and reduction potentials of the solvent and the reactant molecules, as shown in Table 4. The oxidation and reduction potentials of solvents were respectively estimated for DMF, PhCN, DMSO, methyltetrahydrofuran (MTHF), acetonitrile (CH_3CN), ethanol (C_2H_5OH), water (H_2O), and ethyleneglycol (EG) from adiabatic ionization potentials (IP) and electron affinities (EA) in the gas phase by utilizing corrections of the solvent dielectric effect on ionic solvations.[103] Details of the estimations of the ΔG values are described in the Supporting Information. The effective energy gaps (ΔG_{eff}) for solvent oxidation and reduction were obtained from eq 19, as shown in Table 4.

F. Mechanism of Electronic Coupling in Intermolecular ET Systems. In Figure 11, several experimental β values are plotted with respect to the effective energy gap (ΔG_{eff}) for solvent oxidation or reduction listed in Table 4. It is evident from Figure 11 that β strongly depends on ΔG_{eff} and increases with the increase in ΔG_{eff}. This result strongly supports the view that the superexchange, through-solvent mechanism dominates the electronic coupling for long-range intermolecular ET reactions both in the solid[12,63] and liquid solutions. Filled-circle plots were obtained in the present pulsed EPR investigations for the RIP systems (see Table 4). The filled-circle region almost overlaps with the region of the open triangles and open squares ($0.9 \le \beta \le 1.1$ Å^{-1}) reported in the liquid-phase intermolecular ET reactions.[38−41] This result strongly supports the validity of the β determination method using the RPM CIDEP analysis for the solvent-separated RIP systems.

β values have been experimentally determined for the long-range, intrastrand charge-transfer reactions of DNA and have been discussed in terms of the superexchange mechanism.[6,8,9] The superexchange coupling in DNA is regarded as a model of the through-solvent interaction in the intermolecular ET system, since the coupling is dominated by noncovalent bonding interactions[27] through the stacked bases in DNA. $\beta = 0.7$ Å^{-1} was experimentally obtained in hole transfers for a series of strands, $G^+(T)_mGGG \rightarrow G(T)_mGGG^+$,[33,34] where G and T denote guanine and thymine bases, respectively. In this system, $\Delta G_{eff} = 0.66$ eV is obtained with an oxidation potential

TABLE 4: Solvent Ionization Potentials (IP), Electron Affinities (EA), Estimated Oxidation and Reduction Potentials, Effective Energies Gaps (ΔG_{eff}) for Solvent Oxidations and Reductions from the Reactants, and β for Intermolecular ET Reactions in the Condensed Phases

solvent	IP/eV	EA/eV	E^{ox}/ Vvs SCE[m]	E^{red}/ Vvs SCE[n]	reactant	ΔG_{DB}/eV	ΔG_{AB}/eV	ΔG_{eff}/eV	β/Å^{-1}	ref
DMF	9.12[a]	0.01[b]	2.61	−2.50	$DMA^{\bullet+} + DQ^{\bullet-}$	1.71[p]	1.77[q]	1.7	0.91	This work
					$TMB^{\bullet+} + DQ^{\bullet-}$	1.50[p]	1.77[q]	1.5	0.83	
PhCN	9.73[c]	0.26[d]	3.13	−2.48[o]	$ZnP^{\bullet+} + DClQ^{\bullet-}$	2.51[p]	2.33[q]	2.3	0.88	
					$ZnP^{\bullet+} + ClQ^{\bullet-}$	2.51[p]	2.16[q]	2.2	0.96	
					$ZnP^{\bullet+} + XQ^{\bullet-}$	2.51[p]	1.86[q]	1.9	0.97	
					$ZnP^{\bullet+} + DQ^{\bullet-}$	2.51[p]	1.64[q]	1.6	0.87	
DMSO	9.08[e]	−1.93[f]	2.56	−4.48	$TMBD^{\bullet+} + AQ^{\bullet-}$	2.06[p]	3.74[q]	2.1	1.01	
CH_3CN	12.2[g]	0.00[h]	5.21	−2.51	*rhodamine 3B + DMA	3.62[r]	3.41[s]	3.4	1.0	Tavernier et al.[v]
C_2H_5OH	10.4[a]	−2.67[f]	3.83	−5.31	*rhodamine 3B + DMA	2.24[r]	6.34[s]	2.2	1.0	
EG	10.16[i]	−2.33[f]	3.49	−4.89	*CA + DMA	1.93[r]	6.81[s]	1.9	0.9	Murata et al.[w]
					*DCA + ANL	1.60[r]	6.59[s]	1.6	0.9	
					*DCA + ANS	1.60[r]	6.35[s]	1.6	1.1	
					*DCA + DMA	1.60[r]	5.89[s]	1.6	0.9	
2-chlorobutane (77 K)	10.65[j]	N/A	N/A	N/A	$pyrene^{\bullet+} + TMPD$	3.1[j]	4 ∼ 5[j]	3.1	1.16	Miller et al.[x]
MTHF (77 K)	9.22[k]	−2.95[f]	4.37	−7.24	$biphenyl^{\bullet-}$ + fluoranthene	7.62[t]	3.49[u]	3.5	1.23	
H_2O (77 K)	12.62[l]	−2.36[f]	7.67	−7.23	$*Ru(tpy)_2^{2+} + Fe(OH_2)_6^{3+}$	7.03[g]	8.79[t]	7.0	1.68	Ponce et al.[y]

[a] Reference 110. [b] Reference 111. [c] Reference 112. [d] Reference 113. [e] Reference 114. [f] Estimated from EA = $-0.85\epsilon_{LUMO} - 0.91$ (eV). [g] Reference 115. [h] Reference 116. [i] Reference 117. [j] Reference 12. [k] Reference 118. [l] Reference 119. [m] $E^{ox} = E^{ox}_{\epsilon=35.9} - e^2/(4\pi\epsilon_0 a_S) \times (1/\epsilon_S - 1/35.9)$ was used together with $E^{ox}_{\epsilon=35.9} = 0.84 \times IP - 5.04$ (V vs SCE). See Supporting Information for details. [n] $E^{red} = E^{red}_{\epsilon=38.0} + e^2/(4\pi\epsilon_0 a_S) \times (1/\epsilon_S - 1/38.0)$ with $E^{red}_{\epsilon=38.0} = 1.02 \times EA - 2.51$ (V vs SCE) was used. [o] Originating from an electrochemical measurement.[78] [p] Obtained from $\Delta G_{DB} = E^{ox}$(solvent) $- E^{ox}$(donor). [q] $\Delta G_{AB} = E^{red}$(quinone) $- E^{red}$(solvent). [r] Obtained from $\Delta G_{DB} = E^{ox}$(solvent) $- E^{red}$(fluorescer) $- E_{S1}$(fluorescer). [s] Obtained from $\Delta G_{AB} = E^{ox}$(donor) $- E^{red}$(solvent). [t] Obtained from $\Delta G_{DB} = E^{ox}$(solvent) $- E^{red}$(fluoranthene). [u] Obtained from $\Delta G_{AB} = E^{red}$(biphenyl) $- E^{red}$(solvent). [v] References 40 and 41. [w] References 38 and 39. [x] References 12 and 62. [y] Reference 63.

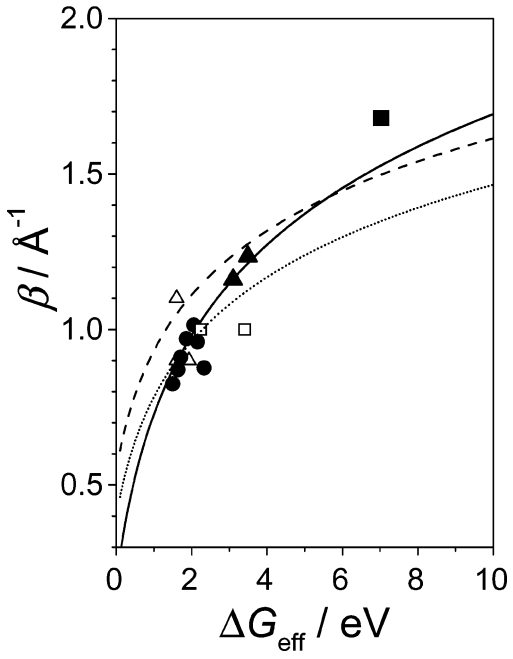

Figure 11. Tunneling energy gap (ΔG_{eff}) dependence of β for intermolecular electron transfers (Table 4): CR in solvent-separated RIPs in this work (●), photoinduced ET from *rhodamine 3B + DMA in ref 40 and 41 (open squares), photoinduced ET from *cyanoanthracenes + donors in ref 38 and 39 (open triangles), charge-transfers in frozen organic solvents in ref 12 and 62 (filled triangles) and photoinduced ET in frozen water in ref 63 (filled square). The dashed and the dotted lines are obtained by superexchange 1D-model of eq 20 with $d_{SS} = 5.7$ Å for $\nu_B = 850$ cm^{-1} (dashed line) and for $\nu_B = 1300$ cm^{-1} (dotted line), respectively. Solid line is obtained by the 3D-model of eq 18 with $d_{SS} = 5.7$ Å and $\nu_B = 850$ cm^{-1}.

difference between T (1.9 V) and G (1.24 V).[32] The superexchange mechanism was also documented in the CS and CR reactions in synthetic DNA hairpins in which an electron acceptor is capped;[6,9] $\beta = 0.66$ Å^{-1} for CS of excited-state *stilbene−(T)$_m$G → stilbene$^-$−(T)$_m$G$^+$ and $\beta = 0.90$ Å^{-1} for CR of stilbene$^-$−(T)$_m$G$^+$ → stilbene−(T)$_m$G were determined.[32] In these systems, $\Delta G_{eff} = 0.5$ and 0.7 eV are estimated for the CS and the CR processes, respectively, using reduction potential (1.44 V) for the excited singlet state of stilbene and from the oxidation potentials of T and G.[32] Surprisingly, comparable β values around 0.9 Å^{-1} are obtained in the solvent-separated RIP systems at much higher energy gaps of $\Delta G_{eff} \approx 1.7$ eV in the present study. This discrepancy can be explained by the difference between the single tunneling pathway in the nucleobase-mediated ET and the multiple solvent-mediated pathways in the intermolecular ET; the multiple pathways enable the long-range features of the electronic couplings and compensate for the disadvantages of the higher tunneling energy gaps. The 3D model mechanism of eq 18 is expected to be applicable to the intermolecular reactions in the condensed phases.

G. Solvent−Solvent Intermolecular Electronic Coupling in the Condensed Phase. To simulate the ΔG_{eff} dependence of β in the intermolecular ET systems, the 1D and the 3D models of the superexchange coupling of eqs 18 and 20 were applied. $d_{SS} = 5.7$ Å can be considered from an averaged value of d_{SS} for the solvent molecules listed in Table 3 except for water. In the solvent-separated RIP systems, total reorganization energies can be estimated from the driving force ($-\Delta G_{CR0}$) under the $P_{RPM} = 0$ conditions.[47,59,60,68] For the DMA−DQ system, $\lambda = 1.63$ eV is obtained from Table 1. For the ZnP−quinone systems, $\lambda = 1.4$ eV is obtained from Figure 8. In frozen MTHF at 77 K, $\lambda = 1.2$ eV was estimated for the long-range ET reactions from the biphenyl anion radicals to the acceptor molecules.[62] In our present analysis, λ was assumed to be 1 eV in eqs 18 and 20 for both liquid and frozen solutions since the distances between the solute and the mediator molecules are shorter than the solute−solute distances (see eq 14). As shown in the solid line in Figure 11, with using $\nu_B = 850$ cm^{-1}, the 3D model of eq 18 accurately reproduces the entire plot except for a filled-square plot for frozen water. The other lines show the 1D model results of eq 20 using $\nu_B = 850$ cm^{-1} (the dashed line) and $\nu_B = 1300$ cm^{-1} (the dotted line) with $d_{SS} = 5.7$ Å. Under the $d_{SS} = 5.7$ Å condition, the 1D model analysis could not reproduce the entire feature of the ΔG_{eff} dependence of β at any ν_B value. The solid line was reproduced when $\nu_B = 2900$ cm^{-1} with $d_{SS} = 4.0$ Å was applied in eq 20. Since $d_{SS} = 4.0$ Å is too short for the mean nearest-neighbor distance of the solvents used in the present study, the 1D model is excluded for the intermolecular ET systems in condensed media. Moreover, the 1D model is unrealistic in the solvent-mediated coupling since the tunneling route cannot be in an exact straight line for any realistic packing scheme. This is consistent with the difference in the tunneling energy gap dependence of β between the intrastrand DNA and the intermolecular ET systems discussed above.

Superexchange couplings have been analyzed for the ET reactions in DNA systems. Voityuk et al.[23] calculated electronic coupling for hole transfers between nearest-neighbor nucleobases at a fixed standard stacking geometry with a rise of 3.38 Å and a twist of 36° in DNA using Hartree−Fock level MO calculations. The superexchange coupling of ν_B(TT) = 1270 cm^{-1} was obtained in the strand G$^+$(T)$_m$GGG. Even though multiple tunneling pathways are taken into account for the condensed phase ET in the present study, a ν_B of 850 cm^{-1} is surprisingly large as an *intermolecular* electronic coupling between randomly oriented solvent molecules at the d_{SS} separation around 5 or 6 Å, compared to a ν_B(TT) of 1270 cm^{-1} induced by the fixed π interaction between the stacked bases separated by 3.4 Å.

Quite recently, the effective electronic coupling in eq 1 has been shown to be dynamically amplified by fluctuating motions of the mediators. Balabin et al.[4] calculated the electron tunneling coupling in the photosynthetic reaction centers at several protein conformations produced by molecular dynamics (MD) simulations. They proposed that electron tunneling is dominated at protein conformations far from equilibrium in the ET reaction from the primary quinone anion ($Q_A^{\bullet -}$) to the secondary quinone of Q_B. Troisi et al.[26] performed the MD simulations of DNA and obtained the time-dependent electronic coupling between the all the pairs of adjacent bases using quantum chemical calculations. The MD results indicated that a quadratic average of the electronic couplings for the DNA hole transfer is 1 or 2 orders of magnitude larger than its mean value because of large fluctuations of the electronic coupling induced by low-frequency motions of the DNA strands.[26] In the condensed-phase intermolecular ET systems, no doubt exists that the solvent molecules undergo the low-frequency intermolecular librations both in the liquid and the frozen solutions. The relatively large through-solvent coupling of $\nu_B = 850$ cm^{-1} is therefore concluded to result from the amplification by the solvent fluctuations and does not reflect a mean value of the couplings averaged by several solvent molecular conformations.[13]

Since d_{SS} (2.8 Å) is much smaller in frozen water solution[104] than in the other solvents as seen in Table 3, the β value (1.68 Å^{-1}) may deviate from the solid line as seen in Figure 11. By application of $d_{SS} = 2.8$ Å to the 3D model of eq 18, the $\beta = 1.68$ Å^{-1} was reproduced when $\nu_B = 3500$ cm^{-1} was set under

the assumption of $\lambda = 1$ eV. Although the large tunneling energy gap ($\Delta G_{\text{eff}} \approx 7$ eV in Table 4) leads to the larger β value in water than in the organic solvents as reported by Ponce et al.,[63] the individual bridge coupling element is estimated here to be more than four times larger in water than in the other solvents. Since several experimental investigations have shown that hydrogen-bond-mediated ET is very efficient,[105−109] the υ_B value of 3500 cm^{-1} may be explained by the coupling via the hydrogen-bond network in frozen water.

III. Conclusion

The main goals of this work were the following: (i) to identify β in eq 2 for charge-recombination in the flexible solvent-separated RIPs in liquid solutions and (ii) to clarify the role of the solvent molecules on the β or V_{DA} for long-range intermolecular ET processes.

We measured the magnitudes of the RPM CIDEP originating from the spin interaction of the 2*J* in the transient RIPs by using the pulsed EPR spectroscopy. To determine β, the RPM CIDEP magnitude was carefully analyzed by the finite-difference calculations of the SLE in which the following effects are taken into account: multiconfiguration interactions from the locally excited states in *J* and the *r*-dependent Coulomb attraction force influencing relative diffusion motions in the RIP.

The β value was strongly dependent on the tunneling energy gap, ΔG_{eff} for solvent oxidation or reduction relative to the reactants. As an example, $\beta = 0.91$ $Å^{-1}$ was determined for CR in the RIP of $DMA^{\bullet+}\cdots DQ^{\bullet-}$ at $\Delta G_{\text{eff}} \sim 1.7$ eV in DMF. This tunneling energy gap is about 1 eV larger than the ΔG_{eff} value that provides the similar β (0.7−0.9 $Å^{-1}$) in the intrastrand charge transfers of DNA duplexes.[32] We concluded that the through-solvent, multiple superexchange pathways enable the long-range features of the electronic couplings, overcoming the disadvantages of the higher tunneling energy gaps. A simple 3D-model of the multiple superexchange couplings mediated by intervening solvent molecules was proposed and adequately explained the ΔG_{eff} dependence of β, including the reported studies in liquid and solid solutions. Nearest-neighbor solvent−solvent electronic coupling was estimated to be 850 cm^{-1} at $d_{SS} \approx 5.7$ Å. This relatively large magnitude of the coupling may be rationalized by the amplification of the low-frequency mediator (solvent−solvent) fluctuations, whose effects are recently reported in the protein-mediated ET of the photosynthetic reaction center[4] and in the nucleobase-mediated long-range charge transfers in DNA.[26]

Our findings indicate that the solvent-mediated superexchange coupling may also play a role for covalently bridged D−A systems at long-distance separations since the β values determined here are quite close to the reported range of $\beta = 0.7$−1.2 $Å^{-1}$ across saturated aliphatic bridges.[16,18−20] From Figure 11, the multiple solvent−solvent tunneling pathways may facilitate ET rather than a single-bonded pathway when ΔG_{eff} is smaller than 1 eV. Solvent-mediated coupling has recently been invoked for some intramolecular ET systems.[13,17] Finally we predict that the solvent redox potential will strongly influence the ET efficiency across the long-range distances, thereby providing insights into the design of systems for photochemical energy conversion.

Appendix. Computation Method of Radical-Pair Mechanism Polarization by SLE

The RPM electron spin polarization is numerically analyzed by the SLE to determine the individual values of β for charge recombination of nanometer-separated RIPs. The effects of the molecular translational diffusion ($\hat{\boldsymbol{\Gamma}}$) and the reaction operator ($\hat{\boldsymbol{K}}$) are included in the SLE analysis. By use of the Laplace transform $\hat{\boldsymbol{\rho}}(r,s)$ of the density matrix of $r\hat{\boldsymbol{\rho}}(r,t)$ in the $S-T_0$ system, the SLE is described as follows[51−53]

$$s\hat{\boldsymbol{\rho}}(r,s) - r\hat{\boldsymbol{\rho}}(r,t=0) = -i[\hat{\boldsymbol{H}}_{\text{RIP}}(r),\hat{\boldsymbol{\rho}}(r,s)] + \hat{\boldsymbol{\Gamma}}\hat{\boldsymbol{\rho}}(r,s) + \hat{\boldsymbol{K}}\hat{\boldsymbol{\rho}}(r,s) \quad \text{(A1)}$$

with

$$\hat{\boldsymbol{\rho}}(r,s) \equiv \int_d^\infty e^{-st} r\hat{\boldsymbol{\rho}}(r,t)\, dt \quad \text{(A2)}$$

$$\hat{\boldsymbol{\rho}}(r,t) = |\psi_{ST_0}\rangle\langle\psi_{ST_0}| \quad \text{(A3)}$$

$$|\psi_{ST_0}\rangle = C_S(r,t)|S\rangle + C_{T_0}(r,t)|T_0\rangle \quad \text{(A4)}$$

The spin Hamiltonian is composed of the Zeemann effect, the exchange *J*, and the hyperfine interaction in the radical pair as

$$\hat{\boldsymbol{H}}_{\text{RIP}}(r) = \beta_e(g_1\hat{\boldsymbol{S}}_1 + g_2\hat{\boldsymbol{S}}_2)\boldsymbol{B}_0 - J(r)\left(2\hat{\boldsymbol{S}}_1\hat{\boldsymbol{S}}_2 + \frac{1}{2}\right) + \sum_m A_{1m}\hat{\boldsymbol{I}}_{1m}\hat{\boldsymbol{S}}_1 + \sum_n A_{2n}\hat{\boldsymbol{I}}_{2n}\hat{\boldsymbol{S}}_2 \quad \text{(A5)}$$

In the system of the RIP with the triplet precursor, since the CR reaction takes place from the singlet RIP to the ground state, $\hat{\boldsymbol{K}}$ is described as

$$\hat{\boldsymbol{K}}\hat{\boldsymbol{\rho}}(r,s) = \frac{-k_{\text{CR}}(r)}{2}\{|S\rangle\langle S|\hat{\boldsymbol{\rho}}(r,s) + \hat{\boldsymbol{\rho}}(r,s)|S\rangle\langle S|\} \quad \text{(A6)}$$

where $k_{\text{CR}}(r)$ is the *r*-dependent charge recombination reaction rate. According to ET theory, $k_{\text{CR}}(r)$ is represented as follows[11,120]

$$k_{\text{CR}}(r) = \left(\frac{\pi}{\hbar^2\lambda_S(r)k_BT}\right)^{1/2} V_{\text{DA}}(r)_G{}^2 \sum_j\{\prod_b \text{FC}_g(j_b)\} \times \exp\left[-\left\{\frac{(\lambda_S(r) - \Delta G_{\text{CR}}(r) + \sum_b j_b h\upsilon_b)^2}{4\lambda_S(r)k_BT}\right\}\right] \quad \text{(A7)}$$

The diffusion motion is represented as follows[51]

$$\hat{\boldsymbol{\Gamma}}\hat{\boldsymbol{\rho}}(r,s) = D\frac{\partial^2}{\partial r^2}\hat{\boldsymbol{\rho}}(r,s) + \frac{D}{r}\left(\frac{\partial}{\partial r}\right)\{F(r)\hat{\boldsymbol{\rho}}(r,s)\} \quad \text{(A8)}$$

with

$$F(r) = \left(\frac{r}{k_BT}\right)\left\{\frac{\partial U(r)}{\partial r}\right\} \quad \text{(A9)}$$

where *D* denotes the mutual diffusion coefficient within the radical pairs. In eq A9, $U(r)$ is the intermolecular interaction potential between the radicals. When $U(r)$ is dominated by Coulomb attraction potential within the solvent-separated RIPs, eq A9 is represented as

$$F(r) = \frac{e^2}{4\pi k_BT\epsilon_0\epsilon_S r} \quad \text{(A10)}$$

By use of the finite difference (Δr) in the distance, eq A8 is rewritten as

$$\hat{\mathbf{\Gamma}}\hat{\boldsymbol{\rho}}(r,s) = \frac{D}{\Delta r^2}\left[\left\{1-\frac{\Delta r_l}{2r_l}F(l)\right\}\hat{\boldsymbol{\rho}}(l-1,s) - \left\{2+\frac{\Delta r_l}{2r_l}\{F(l-1)-F(l+1)\}\right\}\hat{\boldsymbol{\rho}}(l,s) + \left\{1+\frac{\Delta r_l}{2r_l}F(l)\right\}\hat{\boldsymbol{\rho}}(l+1,s)\right] \quad \text{(A11)}$$

where l denotes a site of the distance r. By use of the suitable inner (at $d = 6$ Å) and the outer (at $r_N \approx 100$ Å) boundary conditions of the diffusion matrix $\hat{\boldsymbol{W}}$ and the initial population $\hat{\boldsymbol{\rho}}(t=0)$ of the triplet RIPs, the $\hat{\boldsymbol{\rho}}(s)$ matrix composed of the $4(N+1) \times 4(N+1)$ elements with $l = 0, 1, ..., N$ sites is numerically solved on the basis of eq A1, as follows

$$\hat{\boldsymbol{\rho}}(s) = [s\hat{\boldsymbol{1}} - \hat{\boldsymbol{K}} - \hat{\boldsymbol{W}} + i\hat{\boldsymbol{\Omega}}]^{-1}\hat{\boldsymbol{\rho}}(t=0) \quad \text{(A12)}$$

where

$$\hat{\boldsymbol{\Omega}}(l)\hat{\boldsymbol{\rho}}(l,s) = \begin{pmatrix} 0 & -Q & Q & 0 \\ -Q & 2J(l) & 0 & Q \\ Q & 0 & -2J(l) & -Q \\ 0 & Q & -Q & 0 \end{pmatrix}\begin{pmatrix} \rho_{SS}(l,s) \\ \rho_{ST_0}(l,s) \\ \rho_{T_0S}(l,s) \\ \rho_{T_0T_0}(l,s) \end{pmatrix} \quad \text{(A13)}$$

with

$$2Q = \beta_e(g_1 - g_2)B_0 + \sum_m A_{1m}M_{1m} - \sum_n A_{2n}M_{2n} \quad \text{(A14)}$$

Q can be determined from the g values and hyperfine coupling constants of the ion radicals. For the quinone anion radicals in Table 1, Q values (Q_{+1}) were obtained from differences between the EPR frequencies at the $M_I = +1$ positions and the resonance frequencies at the g values of the countercation radicals.

In $\hat{\boldsymbol{W}}$, we introduced 40 r sites ($N = 40$) composed of the four regions, where each of those possesses 10 sites at a regular interval of Δr_m ($m = 0, 1, 2, 3$). The finite differences were taken at values of $\Delta r_m = f_m \Delta r_{m-1}$ ($m = 1, 2, 3$). For the region of $|J(r)| > |Q|/10$, the intervals were chosen to be small enough by comparing the variation in the $J(r)$ from the adjacent sites. From eq A11 and ref 51, the $\hat{\boldsymbol{W}}$ matrix can be described as follows[51,53]

$$\boldsymbol{W}_{0,0} = -\frac{D}{\Delta r_0^2}\left[2+\frac{\Delta r_0}{d}\{2-F(1)\}\right] \quad \text{(A15)}$$

$$\boldsymbol{W}_{0,1} = \frac{D}{\Delta r_0^2}\left\{2+\frac{\Delta r_0}{d}F(0)\right\} \quad \text{(A16)}$$

$$\boldsymbol{W}_{l,l-1} = \frac{D}{\Delta r_m^2}\left\{1-\frac{\Delta r_m}{2r_l}F(l)\right\} \quad \text{(A17)}$$

$$\boldsymbol{W}_{l,l} = -\frac{2D}{\Delta r_m^2}\left[2+\frac{\Delta r_m}{2r_l}\{F(l-1)-F(l+1)\}\right] \quad \text{(A18)}$$

$$\boldsymbol{W}_{l,l+1} = \frac{D}{\Delta r_m^2}\left\{1+\frac{\Delta r_m}{2r_l}F(l)\right\} \quad \text{(A19)}$$

with $l > 0$ except for $l = 10m$ ($m = 1, 2, 3$). And, for $M = 10m$ ($m = 1, 2, 3$)

$$\boldsymbol{W}_{M,M-1} = \frac{2D}{\Delta r_{m-1}^2(1+f_m)}\left\{1-\frac{\Delta r_{m-1}}{2r_M}F(M)\right\} \quad \text{(A20)}$$

$$\boldsymbol{W}_{M,M} = -\frac{D}{\Delta r_{m-1}^2}\left\{\frac{2}{f_m}+\frac{\Delta r_{m-1}}{r_M(1+f_m)}F(M-1) - \frac{\Delta r_{m-1}}{r_M f_m(1+f_m)}F(M+1)\right\} \quad \text{(A21)}$$

$$\boldsymbol{W}_{M,M+1} = \frac{2D}{\Delta r_{m-1}^2 f_m(1+f_m)}\left\{1+\frac{\Delta r_{m-1}}{2r_M}F(M)\right\} \quad \text{(A22)}$$

Finally

$$\boldsymbol{W}_{N-1,N} = 0 \quad \text{(A23)}$$

$$\boldsymbol{W}_{N,N-1} = \frac{2D}{f_3^2\Delta r_2^2} \quad \text{(A24)}$$

$$\boldsymbol{W}_{N,N} = 0 \quad \text{(A25)}$$

In the present study, the following values were employed for the finite-difference analysis: $\Delta r_0 = 0.4$ Å, $f_1 = {}^3/_4$, $f_2 = {}^8/_3$, and $f_3 = 10$. We also checked the numerical computations by reducing the finite-difference values of Δr; $N = 80$, $M = 20m$ ($m = 1, 2, 3$), $\Delta r_0 = 0.2$ Å, $f_1 = {}^3/_4$, $f_2 = {}^8/_3$, and $f_3 = 10$. The computational results were confirmed not to be changed from those obtained under the $N = 40$ conditions for $0.9 < \beta < 1.2$ Å^{-1}.

The mutual translational diffusion coefficients were obtained by the Stokes−Einstein relationship as follows

$$D = \frac{k_B T}{6\pi\eta}\left(\frac{1}{d_D}+\frac{1}{d_A}\right) \quad \text{(A26)}$$

where η is the solvent viscosity. Recent transient grating studies by Okamoto et al. have experimentally revealed that the diffusion coefficients of cation and anion transient radicals agree with the Stokes−Einstein formula.[121,122] $\eta(T)_{DMF} = 2.76 \times 10^{-2}$ exp(1029/T) cP was obtained from reported viscosity values at several temperatures. $\eta(273\text{ K})_{PhCN} = 1.94$ cP and $\eta(295\text{ K})_{DMSO} = 2.4$ cP[78] were utilized. D values are listed in Table 2.

The calculated RPM polarization P_{RPM} on radical 1 is obtained from the computed density matrix by the following relation[51]

$$P_{RPM} = -2\lim_{s\to 0} s\int_d^{r_N} tr\{r\hat{\boldsymbol{\rho}}(r,s)\hat{\boldsymbol{S}}_{1Z}\}\,dr = -2\lim_{s\to 0} s\sum_l^N r_l\Delta r_l\rho_{ST_0}(l,s) \quad \text{(A27)}$$

The initial condition of the density matrix $\hat{\boldsymbol{\rho}}$ ($t = 0$) can be assumed to be dominated at the closest distance d by the T_0 state as $\rho_{T_0,T_0}(r,t=0) = \rho_0\delta(r-d)/3d^2$ since the photoinduced CS reactions have been shown to take place via the exciplex or the contact RIPs in the intermolecular D−A systems.[48,70,73,123] This assumption for the initial conditions is valid when $\Delta G_{CS} > -1$ eV for the forward ET reactions.[124]

Inclusion of the effect of the long-range Coulomb attraction field $F(r)$ has been found to affect the magnitude of calculated P_{RPM} in this study; P_{RPM} magnitudes became smaller by 30−40% than P_{RPM} values calculated without taking account the

$F(r)$ effects when $\beta = 1.0$ Å^{-1} is utilized in the polar solvents. This result may be consistent with the theoretical studies predicted by Pedersen et al.[51] In addition to the Coulomb field effect, solvation structure due to a potential of mean force of $U(r) = -k_BT \ln\{g(r)\}$ is known to influence the mutual diffusional motions.[40] $g(r)$ represents a hard-sphere radial distribution function and has been represented by solute−solute, solvent−solute, and solvent−solvent interactions by means of the Lennard-Jones (LJ) potentials.[80] The $g(r)$ effect was however neglected in this study since the LJ field is effective around short-range distance of $r \approx 7$ Å and is less effective than the long-range Coulomb potential in the RIP systems especially for the effective CIDEP generation distance of $r_{eff} = 12$ Å (when $\beta = 1.0$ Å^{-1}).[41,59,60,80] A potential surface effect of the $J(r)$[51] on the diffusion motion is also ignored in eq A9 since the computed J energies ($\sim 10^{12}$ rad/s) are much smaller than the thermal energy of k_BT even at the separation of d.

Recent time-resolved fluorescence-measurement studies suggested that the mutual diffusion coefficient D is dependent on the intermolecular distance r because of hydrodynamic (HD) effects;[40,94] inclusion of the HD effects explained well the nonexponential features of fluorescence-quenching intermolecular ET reactions. In the present study, the HD effect was not taken into account in the SLE. Pedersen et al.[53] investigated the HD effect on RPM CIDEP using finite-difference analysis and concluded that the effect is negligible in the case of $J_0 > 10^{11}$ rad/s with $\alpha \approx 3.0$ Å^{-1} in $J_{EX}(r) = J_0 \exp\{-\alpha(r - d)\}$. In the present study, since magnitudes of $|2J(d)|$ are large enough as shown in Figure 7 and β (<1 Å^{-1}) is much smaller than the α of 3.0 Å^{-1} of the previous investigation,[53] the HD effect will be much less important. This is because r_{eff} (>12 Å) is too long for the HD effect to influence the diffusional motions in the solvent-separated RIPs, while the HD effect has a significant role on the time dependence of the ET quenching that dominates near-contact separations.[40,41,94]

Acknowledgment. Support from the U. S. Department of Energy, Office of Basic Energy Sciences, Division of Chemical Sciences Contract DE-FG02-96ER14675 is gratefully acknowledged. Y.K. is grateful to the Japan Society of the Promotion of Science for postdoctoral fellowships of research abroad.

Supporting Information Available: Derivations of eqs 3 and 4 and examples of the electrochemical measurements and determinations of the oxidation and reduction potentials of DMA and DQ are shown. The method of the calculations of the energy gaps (Table 4) for solvent oxidation and reduction from reactant molecules are described. This material is available free of charge via the Internet at http://pubs.acs.org.

References and Notes

(1) Page, C. C.; Moser, C. C.; Chen, X. X.; Dutton, P. L. *Nature* **1999**, *402*, 47.
(2) Sikes, H. D.; Smalley, J. F.; Dudek, S. P.; Cook, A. R.; Newton, M. D.; Chidsey, C. E. D.; Feldberg, S. W. *Science* **2001**, *291*, 1519.
(3) Galoppini, E.; Guo, W. Z.; Qu, P.; Meyer, G. J. *J. Am. Chem. Soc.* **2001**, *123*, 4342.
(4) Balabin, I. A.; Onuchic, J. N. *Science* **2000**, *290*, 114.
(5) Kelley, S. O.; Barton, J. K. *Science* **1999**, *283*, 375.
(6) Lewis, F. D.; Wu, T. F.; Zhang, Y. F.; Letsinger, R. L.; Greenfield, S. R.; Wasielewski, M. R. *Science* **1997**, *277*, 673.
(7) Lancaster, C. R. D.; Kroger, A.; Auer, M.; Michel, H. *Nature* **1999**, *402*, 377.
(8) Giese, B.; Amaudrut, J.; Kohler, A. K.; Spormann, M.; Wessely, S. *Nature* **2001**, *412*, 318.
(9) Lewis, F. D.; Liu, X. Y.; Liu, J. Q.; Miller, S. E.; Hayes, R. T.; Wasielewski, M. R. *Nature* **2000**, *406*, 51.
(10) Marcus, R. A. *J. Chem. Phys.* **1956**, *24*, 966.
(11) Marcus, R. A.; Sutin, N. *Biochim. Biophys. Acta* **1985**, *811*, 265.
(12) Miller, J. R.; Beitz, J. V. *J. Chem. Phys.* **1981**, *74*, 6746.
(13) Zimmt, M. B.; Waldeck, D. H. *J. Phys. Chem. A* **2003**, *107*, 3580.
(14) Miller, J. R. *Science* **1975**, *189*, 221.
(15) McConnel, H. *J. Chem. Phys.* **1961**, *35*, 508.
(16) Penfield, K. W.; Miller, J. R.; Paddonrow, M. N.; Cotsaris, E.; Oliver, A. M.; Hush, N. S. *J. Am. Chem. Soc.* **1987**, *109*, 5061.
(17) Lukas, A. S.; Bushard, P. J.; Wasielewski, M. R. *J. Phys. Chem. A* **2002**, *106*, 2074.
(18) Paddon-Row, M. N.; Shephard, M. J. *J. Phys. Chem. A* **2002**, *106*, 2935.
(19) Johnson, M. D.; Miller, J. R.; Green, N. S.; Closs, G. L. *J. Phys. Chem.* **1989**, *93*, 1173.
(20) Closs, G. L.; Miller, J. R. *Science* **1988**, *240*, 440.
(21) Bixon, M.; Giese, B.; Wessely, S.; Langenbacher, T.; Michel-Beyerle, M. E.; Jortner, J. *Proc. Natl. Acad. Sci. U. S. A.* **1999**, *96*, 11713.
(22) Bixon, M.; Jortner, J. *J. Phys. Chem. B* **2000**, *104*, 3906.
(23) Voityuk, A. A.; Rosch, N.; Bixon, M.; Jortner, J. *J. Phys. Chem. B* **2000**, *104*, 9740.
(24) Voityuk, A. A.; Jortner, J.; Bixon, M.; Rosch, N. *Chem. Phys. Lett.* **2000**, *324*, 430.
(25) Voityuk, A. A.; Jortner, J.; Bixon, M.; Rosch, N. *J. Chem. Phys.* **2001**, *114*, 5614.
(26) Troisi, A.; Orlandi, G. *J. Phys. Chem. B* **2002**, *106*, 2093.
(27) Tong, G. S. M.; Kurnikov, I. V.; Beratan, D. N. *J. Phys. Chem. B* **2002**, *106*, 2381.
(28) Jortner, J.; Bixon, M.; Voityuk, A. A.; Rosch, N. *J. Phys. Chem. A* **2002**, *106*, 7599.
(29) Bixon, M.; Jortner, J. *Chem. Phys.* **2002**, *281*, 393.
(30) Porath, D.; Bezryadin, A.; de Vries, S.; Dekker, C. *Nature* **2000**, *403*, 635.
(31) Bixon, M.; Jortner, J. *J. Am. Chem. Soc.* **2001**, *123*, 12556.
(32) Lewis, F. D.; Letsinger, R. L.; Wasielewski, M. R. *Acc. Chem. Res.* **2001**, *34*, 159.
(33) Meggers, E.; Michel-Beyerle, M. E.; Giese, B. *J. Am. Chem. Soc.* **1998**, *120*, 12950.
(34) Meggers, E.; Kusch, D.; Spichty, M.; Wille, U.; Giese, B. *Angew. Chem., Int. Ed.* **1998**, *37*, 460.
(35) Onuchic, J. N.; Beratan, D. N. *J. Chem. Phys.* **1990**, *92*, 722.
(36) Regan, J. J.; Risser, S. M.; Beratan, D. N.; Onuchic, J. N. *J. Phys. Chem.* **1993**, *97*, 13083.
(37) Langen, R.; Chang, I. J.; Germanas, J. P.; Richards, J. H.; Winkler, J. R.; Gray, H. B. *Science* **1995**, *268*, 1733.
(38) Murata, S.; Matsuzaki, S. Y.; Tachiya, M. *J. Phys. Chem.* **1995**, *99*, 5354.
(39) Murata, S.; Tachiya, M. *J. Phys. Chem.* **1996**, *100*, 4064.
(40) Tavernier, H. L.; Kalashnikov, M. M.; Fayer, M. D. *J. Chem. Phys.* **2000**, *113*, 10191.
(41) Tavernier, H. L.; Fayer, M. D. *J. Chem. Phys.* **2001**, *114*, 4552.
(42) Langen, R.; Colon, J. L.; Casimiro, D. R.; Karpishin, T. B.; Winkler, J. R.; Gray, H. B. *J. Biol. Inorg. Chem.* **1996**, *1*, 221.
(43) Anderson, P. W. *Phys. Rev.* **1959**, *115*, 2.
(44) Bixon, M.; Jortner, J.; Michelbeyerle, M. E. *Phys. Chem. Chem. Phys.* **1993**, *180*, 193.
(45) Volk, M.; Haberle, T.; Feick, R.; Ogrodnik, A.; Michelbeyerle, M. E. *J. Phys. Chem.* **1993**, *97*, 9831.
(46) Sekiguchi, S.; Kobori, Y.; Akiyama, K.; Tero-Kubota, S. *J. Am. Chem. Soc.* **1998**, *120*, 1325.
(47) Kobori, Y.; Akiyama, K.; Tero-Kubota, S. *J. Chem. Phys.* **2000**, *113*, 465.
(48) Kobori, Y.; Sekiguchi, S.; Akiyama, K.; Tero-Kubota, S. *J. Phys. Chem. A* **1999**, *103*, 5416.
(49) Lukas, A. S.; Bushard, P. J.; Weiss, E. A.; Wasielewski, M. R. *J. Am. Chem. Soc.* **2003**, *125*, 3921.
(50) Muss, L. T.; Atkins, P. W.; McLauchlan, K. A.; Pedersen, J. B. *Chemically Induced Magnetic Polarization*; Reidel: Dordrecht, The Netherlands, 1977.
(51) Pedersen, J. B.; Freed, J. H. *J. Chem. Phys.* **1973**, *59*, 2869.
(52) Pedersen, J. B.; Freed, J. H. *J. Chem. Phys.* **1973**, *58*, 2746.
(53) Pedersen, J. B.; Freed, J. H. *J. Chem. Phys.* **1975**, *62*, 1790.
(54) Vanwilligen, H.; Levstein, P. R.; Ebersole, M. H. *Chem. Rev.* **1993**, *93*, 173.
(55) Adrian, F. J. *J. Chem. Phys.* **1970**, *53*, 3374.
(56) Adrian, F. J. *J. Chem. Phys.* **1971**, *54*, 3912.
(57) Adrian, F. J. *J. Chem. Phys.* **1971**, *54*, 3918.
(58) Adrian, F. J. *J. Chem. Phys.* **1972**, *57*, 5107.
(59) Yago, T.; Kobori, Y.; Akiyama, K.; Tero-Kubota, S. *J. Phys. Chem. B* **2002**, *106*, 10074.
(60) Kobori, Y.; Yago, T.; Akiyama, K.; Tero-Kubota, S. *J. Am. Chem. Soc.* **2001**, *123*, 9722.
(61) Kobori, Y.; Yago, T.; Tero-Kubota, S. *Appl. Magn. Reson.* **2003**, *23*, 269.

(62) Miller, J. R.; Beitz, J. V.; Huddleston, R. K. *J. Am. Chem. Soc.* **1984**, *106*, 5057.
(63) Ponce, A.; Gray, H. B.; Winkler, J. R. *J. Am. Chem. Soc.* **2000**, *122*, 8187.
(64) Segal, B. G.; Kaplan, M.; Fraenkel, G. K. *J. Chem. Phys.* **1965**, *43*, 4191.
(65) Nagaoka, S.; Ishihara, K. *J. Am. Chem. Soc.* **1996**, *118*, 7361.
(66) Atkins, P. W.; Evans, G. T. *Mol. Phys.* **1975**, *29*, 921.
(67) Pedersen, J. B.; Freed, J. H. *J. Chem. Phys.* **1975**, *62*, 1706.
(68) Yago, T.; Kobori, Y.; Akiyama, K.; Tero-Kubota, S. *Chem. Phys. Lett.* **2003**, *369*, 49.
(69) Batchelor, S. N.; Heikkila, H.; Kay, C. W. M.; McLauchlan, K. A.; Shkrob, I. A. *Chem. Phys.* **1992**, *162*, 29.
(70) Sasaki, S.; Kobori, Y.; Akiyama, K.; Tero-Kubota, S. *J. Phys. Chem. A* **1998**, *102*, 8078.
(71) Kobori, Y.; Takeda, K.; Tsuji, K.; Kawai, A.; Obi, K. *J. Phys. Chem. A* **1998**, *102*, 5160.
(72) Savitsky, A. N.; Paul, H.; Shushin, A. I. *J. Phys. Chem. A* **2000**, *104*, 9091.
(73) Tachikawa, T.; Kobori, Y.; Akiyama, K.; Katsuki, A.; Steiner, U. E.; Tero-Kubota, S. *Chem. Phys. Lett.* **2002**, *360*, 13.
(74) Levstein, P. R.; Vanwilligen, H. *J. Chem. Phys.* **1991**, *95*, 900.
(75) Ebersole, M.; Levstein, P. R.; Vanwilligen, H. *J. Phys. Chem.* **1992**, *96*, 9310.
(76) Jager, M.; Norris, J. R. *J. Phys. Chem. A* **2002**, *106*, 3659.
(77) Fujisawa, J.; Ohba, Y.; Yamauchi, S. *Chem. Phys. Lett.* **1998**, *294*, 248.
(78) Murov, S. L.; Carmichael, I.; Hug, G. L. *Handbook of Photochemistry*, 2nd ed.; Marcel Dekker: New York, 1993.
(79) Calvo, R.; Abresch, E. C.; Bittl, R.; Feher, G.; Hofbauer, W.; Isaacson, R. A.; Lubitz, W.; Okamura, M. Y.; Paddock, M. L. *J. Am. Chem. Soc.* **2000**, *122*, 7327.
(80) Kitahama, Y.; Kimura, Y.; Hirota, N. *Bull. Chem. Soc. Jpn.* **2000**, *73*, 851.
(81) Vath, P.; Zimmt, M. B.; Matyushov, D. V.; Voth, G. A. *J. Phys. Chem. B* **1999**, *103*, 9130.
(82) Davis, W. B.; Ratner, M. A.; Wasielewski, M. R. *J. Am. Chem. Soc.* **2001**, *123*, 7877.
(83) Sato, H.; Kobori, Y.; Tero-Kubota, S.; Hirata, F. *J. Chem. Phys.* **2003**, *119*, 2753.
(84) Vath, P.; Zimmt, M. B. *J. Phys. Chem. A* **2000**, *104*, 2626.
(85) Marcus, Y. *Introduction to Liquid-State Chemistry*; Wiley & Sons: New York, 1977.
(86) Budavari, S. *The Merck Index: An Encyclopedia of Chemicals, Drugs and Biologicals*, 11th ed.; Merck & Co.: Rathway, NJ, 1989.
(87) Riddick, J.; Bunger, W. B. *Organic Solvents; Physical Properties and Methods of Purification*, 3rd ed.; Wiley-Interscience: New York, 1970.
(88) Weast, R. C. *CRC Handbook of Chemistry and Physics*; CRC Press: Boca Raton, FL, 1995.
(89) Nagaoka, S.; Ishihara, K. *J. Am. Chem. Soc.* **1996**, *118*, 7361.
(90) Zelent, B.; Kusba, J.; Gryczynski, I.; Johnson, M. L.; Lakowicz, J. R. *J. Phys. Chem.* **1996**, *100*, 18592.
(91) Herre, W.; Weis, P. *Spectrochim. Acta* **1973**, *29A*, 203.
(92) Tung, C.; Zhang, L.; Li, Y.; Cao, H.; Tanimoto, Y. *J. Am. Chem. Soc.* **1997**, *119*, 5348.
(93) Ganesan, V.; Rosokha, S. V.; Kochi, J. K. *J. Am. Chem. Soc.* **2003**, *125*, 2559.
(94) Tavernier, H. L.; Laine, F.; Fayer, M. D. *J. Phys. Chem. A* **2001**, *105*, 8944.
(95) Balakrishnan, G.; Keszthelyi, T.; Wilbrandt, R.; Zwier, J. M.; Brouwer, A. M.; Buma, W. J. *J. Phys. Chem. A* **2000**, *104*, 1834.
(96) Sakanoue, K.; Motoda, M.; Sugimoto, M.; Sakaki, S. *J. Phys. Chem. A* **1999**, *103*, 5551.
(97) Khandelwal, S. C.; Roebber, J. L. *Chem. Phys. Lett.* **1975**, *34*, 355.
(98) Nakato, Y.; Abe, K.; Tsubomura, H. *Chem. Phys. Lett.* **1976**, *39*, 358.
(99) Gould, I. R.; Young, R. H.; Mueller, L. J.; Albrecht, A. C.; Farid, S. *J. Am. Chem. Soc.* **1994**, *116*, 3147.
(100) On the P_{RPM} calculations, the γ value was found to be sensitive only for $P_{RPM} \approx 0$ conditions. In the calculated lines in Figure 8, $\gamma = 1.03$ is also applicable in $d_D = 6.2$ Å and $d_A = 3.7$ Å because $a_D = 6.02$ Å and $a_A = 3.58$ Å in ZnP and DQ, respectively. For simulations of the absolute magnitudes of the P_{RPM} values larger than 1 P_{eq}, the γ value was not so sensitive. When $\gamma = 1.000$ was applied for the analysis of the ZnP−ClQ system in PhCN, as an example, deviation of β was only 0.01 Å^{-1} ($\beta = 0.98$ Å^{-1}) to reproduce the experimental $P_{RPM}(+1)$ value of 12 P_{eq}.
(101) Cordeiro, J. M. M. *Int. J. Quantum Chem.* **1997**, *65*, 709.
(102) Koga, Y.; Kasahara, Y.; Yoshino, K.; Nishikawa, K. *J. Solution Chem.* **2001**, *30*, 885.
(103) Gaines, G. L.; Oneil, M. P.; Svec, W. A.; Niemczyk, M. P.; Wasielewski, M. R. *J. Am. Chem. Soc.* **1991**, *113*, 719.
(104) Klug, D. D.; Mishima, O.; Whalley, E. *J. Chem. Phys.* **1987**, *86*, 5323.
(105) Wuttke, D. S.; Bjerrum, M. J.; Winkler, J. R.; Gray, H. B. *Science* **1992**, *256*, 1007.
(106) Babini, E.; Bertini, I.; Borsari, M.; Capozzi, F.; Luchinat, C.; Zhang, X. Y.; Moura, G. L. C.; Kurnikov, I. V.; Beratan, D. N.; Ponce, A.; Di Bilio, A. J.; Winkler, J. R.; Gray, H. B. *J. Am. Chem. Soc.* **2000**, *122*, 4532.
(107) Kirby, J. P.; Roberts, J. A.; Nocera, D. G. *J. Am. Chem. Soc.* **1997**, *119*, 9230.
(108) Yang, J.; Seneviratne, D.; Arbatin, G.; Andersson, A. M.; Curtis, J. C. *J. Am. Chem. Soc.* **1997**, *119*, 5329.
(109) Derege, P. J. F.; Williams, S. A.; Therien, M. J. *Science* **1995**, *269*, 1409.
(110) Watanabe, K.; Nakayama, T.; Mottl, J. *J. Quant. Spectrosc. Radiat. Transfer* **1962**, *2*, 369.
(111) Desfrancois, C.; Periquet, V.; Carles, S.; Schermann, J. P.; Smith, D. M. A.; Adamowicz, L. *J. Chem. Phys.* **1999**, *110*, 4309.
(112) Araki, M.; Sato, S. *J. Phys. Chem.* **1996**, *100*, 10542.
(113) Wentworth, W. E.; Kao, L. W.; Becker, R. S. *J. Phys. Chem.* **1975**, *79*, 1161.
(114) Potzinger, P.; Stracke, H.-U.; Kupper, W.; Gollnick, K. *Z. Naturforsch. A* **1975**, *30*, 340.
(115) Gochel-Dupuis, M.; Delwiche, J.; Hubin-Franskin, M.-J.; Collin, J. E. *Chem. Phys. Lett.* **1992**, *193*, 41.
(116) Bailey, C. G.; Dessent, C. E. H.; Johnson, M. A.; Bowen, K. A. *J. Chem. Phys.* **1996**, *104*, 6976.
(117) Holmes, J. L.; Lossing, F. P. *Can. J. Chem.* **1982**, *60*, 2365.
(118) Holmes, J. L.; Lossing, F. P. *Org. Mass Spectrom.* **1991**, *26*, 537.
(119) Reutt, J. E.; Wang, L. S.; Lee, Y. T.; Shirley, D. A. *J. Chem. Phys.* **1986**, *85*, 6928.
(120) Hopfield, J. J. *Proc. Natl. Acad. Sci. U. S. A.* **1974**, *71*, 3640.
(121) Terazima, M.; Okazaki, T.; Hirota, N. *J. Photochem. Photobiol., A* **1995**, *92*, 7.
(122) Okamoto, K.; Hirota, N.; Terazima, M. *J. Chem. Soc., Faraday Trans.* **1998**, *94*, 185.
(123) Tachikawa, T.; Kobori, Y.; Akiyama, K.; Katsuki, A.; Usui, Y.; Steiner, U. E.; Tero-Kubota, S. *Mol. Phys.* **2002**, *100*, 1413.
(124) Tachiya, M.; Murata, S. *J. Phys. Chem.* **1992**, *96*, 8441.